AMPK signaling in dendritic cells: a metabolic sensor controlling the balance between immunity and tolerance

Brombacher, E.C.


AMPK

6

AMPK activation in tumor-associated dendritic cells promotes tumor growth

E. C. Brombacher[1], T. A. Patente[1], F. Otto[1], M. Quik[1], G. A. Heieis[1], L. P. Almeida[1], J. M. Lambooij[1], R. Arens[2], B. Everts[1]

[1]Department of Parasitology, Leiden University Medical Center, Leiden, The Netherlands
[2]Department of Immunology, Leiden University Medical Center, Leiden, The Netherlands

Manuscript in preparation

Abstract

Dendritic cells (DCs) in tumors are often less immunogenic and are commonly exposed to a nutrient poor tumor microenvironment (TME). Several studies indicate that tolerogenicity of DCs is dependent on engagement of catabolic metabolism. An important upstream metabolic sensor that promotes catabolic metabolism under nutrient-deprived conditions is AMP-activated kinase (AMPK). Yet whether or how AMPK activation controls tolerogenicity of tumor-associated (TA)-DCs in the TME is still not known. Here we found that TA-DCs displayed enhanced AMPK activity in a murine melanoma model. Mice with a selective deficiency of AMPKα1 in DCs were better capable of controlling melanoma tumor growth than their wild-type littermates. AMPKα1-deficiency in TA-cDC1s induced accumulation of GLUT1^{+} cDC1s and promoted CD86 expression, suggesting that loss of AMPKα1, may render DCs more immunogenic. Correspondingly, tumor-infiltrating CD8^{+} T cells expressed higher levels of TNF in CD11c$^{\Delta AMPK\alpha1}$ mice when compared to CD11c^{WT} mice. Metabolically, loss of AMPKα1 particularly boosted expression of acetyl-CoA carboxylase-1 (ACC1), a key enzyme in fatty acid synthesis, in TA-DCs. Functionally, inhibition of ACC activity did not affect CD8^{+} T cell priming by TA-DCs, but instead it potentiated their ability to induce regulatory T cells *ex vivo*, suggesting that this pathway may control tolerogenicity in TA-DCs. While the exact immunological effector mechanisms that drive tumor progression downstream of AMPK signaling in DCs remain to be explored, our findings reveal a key role for AMPK-signaling in shaping DC immunogenicity with possible implication for the treatment of malignancies.

Introduction

Tumor cells require significant amounts of energy and nutrients for growth and proliferation. Oncogenic signals induce metabolic rewiring to meet the bioenergetic and biosynthetic needs of malignant cells, which leads to metabolic stress for other cells residing in the same tumor microenvironment (TME), including immune cells. Cancer cells induce an immunosuppressive environment by shaping a metabolically heterogenous TME with hypoxic regions, low nutrient availability, and accumulation of metabolic waste products (1,2). A major sensor of such metabolic stress is AMP-activated protein kinase (AMPK), which maintains energy homeostasis in nutrient-stressful conditions (3). Interestingly, AMPK activation is also known to have anti-inflammatory effects (4) and could therefore provide a link between a nutrient restricted micro-environment and suppression of tumor-infiltrating immune cells.

Dendritic cells (DCs), in particular type 1 conventional DCs (cDC1s) (5), are critical for the anti-tumor immune response and hence there is significant interest in targeting DCs for antitumor immunotherapies (6). This includes targeted delivery of antigens and adjuvants to DCs as well as *ex vivo* loading of tumor-derived DCs or monocyte-derived DCs with tumor antigens (6,7). However, DCs residing in the TME are often compromised in function due to immunosuppressive tumor-derived factors and this has yet to be overcome (8). Thus far little is known about the role of AMPK in driving immune suppression in tumor-associated DCs (TA-DCs). AMPK activation was previously shown to suppress LPS-induced DC activation (9,10) and we recently observed that AMPK signaling can induce tolerogenic DCs that promote priming of regulatory T cells (Chapter 5). Interestingly, increased expression of canonical AMPK activator liver kinase B1 (LKB1) in TA-DCs (11), may point towards increased signaling of the LKB1-AMPK axis in these cells. If AMPK activation is indeed enhanced in TA-DCs and whether this compromises DC immunogenicity remains to be explored.

In other TA-immune cells this has been studied in more detail. For instance, myeloid-derived suppressor cells (MDSCs) (12) and regulatory T cells (Tregs) (13) in various murine tumors show increased AMPK activation and total protein abundance, respectively, when compared to their splenic counterparts. AMPKα1-deficiency in MDSCs improves anti-tumor cytotoxicity and reduces tumor development (12), as does Treg-specific AMPKα1-deficiency (13). On the contrary, a decrease in total AMPK accumulation is also observed for Tregs in B16F10 melanoma compared to peripheral Tregs in tumor-free mice (14) and AMPK loss in the total T cell pool supports tumor growth, due to enhanced T cell death and a reduction in $CD8^+$ T cell activation (15). This highlights an important role for AMPK signaling in shaping the biology of various immune cells in the TME.

Here, we investigated whether this also applies to TA-DCs by assessing if the TME alters AMPK activity and thereby their functional properties. We show that TA-DCs from murine melanomas display increased AMPK activity compared to splenic DCs. Mice deficient for AMPK in CD11c-expressing cells showed reduced tumor growth, suggesting heightened AMPK activation in TA-DCs contributes to impaired anti-tumor immune responses.

Results

AMPK activation in TA-DCs promotes tumor growth

To investigate whether AMPK activity is induced in immune cells residing in an immunosuppressive, nutrient-limited TME, we inoculated mice subcutaneously with highly

glycolytic B16F10 OVA-expressing melanoma cells (16) and analyzed the phosphorylation of AMPK-specific phosphorylation site S79 on ACC (pACC) using flow cytometry (17). Interestingly, tumor-infiltrating immune cells (gating strategy provided in Supp. Fig. 1A-D), including TA-cDC1s, showed increased levels of pACC compared to their spleen-derived counterparts (Fig. 1A). Similarly, immune cells in the tumor draining lymph node (TDLN) exhibited higher pACC signal compared to their counterparts in the contralateral non-draining lymph node (NDLN) (Fig. 1B), altogether indicating increased AMPK activation in tumor-associated immune cells. To study whether this increased AMPK signaling specifically in DCs affects the anti-tumor immune response, we compared tumor growth in mice with a Cre-induced deletion of AMPKα1 in CD11c-expressing cells ($CD11c^{\Delta AMPK\alpha1}$) to Cre-negative AMPK sufficient littermates ($CD11c^{WT}$). We confirmed the specificity of the model by showing there was a DC-specific decrease in AMPK signaling in splenocytes from $CD11c^{\Delta AMPK\alpha1}$ mice (Fig. 1C). Of note, the decrease in pACC signal in $CD11c^{\Delta AMPK\alpha1}$ DCs differed between tissues and was less pronounced in TA-cDC2s and NDLN-cDC2s (Supp. Fig. 2A). Although there was a trend towards reduced kinetics in tumor growth in $CD11c^{\Delta AMPK\alpha1}$ mice this did not reach statistical significance (Fig. 1D), However, there was significant lower tumor weight in $CD11c^{\Delta AMPK\alpha1}$ mice at the time of sacrifice, 3 weeks after inoculation (Fig. 1E, F). Together this suggests that heightened AMPK signaling in TA-DCs compromises control of tumor growth.

CD86 expression by cDC1s is suppressed by AMPK activation

To explore potential mechanisms underlying the reduced tumor growth in $CD11c^{\Delta AMPK\alpha1}$ mice, we next determined how AMPK activation affects DC abundance and phenotype within the tumor and TDLNs. Tumor-infiltrating leukocyte numbers (Fig. 2A) and the frequency of total cDCs or DC subsets within the tumor (Fig. 2B,C) or TDLN (Supp. Fig. 2B,C) were not affected by loss of AMPKα1 in DCs. Abundance of other myeloid populations within the tumor were also not different between $CD11c^{WT}$ and $CD11c^{\Delta AMPK\alpha1}$ mice (Supp. Fig. 2D). AMPKα1-deficiency induced an increase in CD86 expression in TA- and TDLN cDC1s (Fig. 2D, Supp. Fig. 2E), while activation status of cDC2s remained unchanged (Fig. 2E and Supp. Fig. 2F). Regulatory markers PD-L1, indoleamine-pyrrool 2,3-dioxygenase (IDO) (8), and TIM3 (18) (Fig. 2D, E), and immunosuppressive retinaldehyde dehydrogenase (RALDH) activity (19) (Fig. 2F,G) did not change upon AMPKα1-deficiency in neither cDC1s nor cDC2s and expression levels of cytokines were also not affected after *ex vivo* stimulation with LPS and CpG in the presence of Brefeldin A in neither tumor (Fig. 2H,I) nor TDLN DCs (Supp. Fig. 2G,H). Of note, a subset of macrophages also expresses CD11c (Supp. Fig. 3A), and consistent with no differences in pACC levels in total splenic macrophages (Fig. 1C), AMPK signaling did not differ in tumor-associated macrophages of $CD11c^{\Delta AMPK\alpha1}$ mice compared to $CD11c^{WT}$ mice (Supp. Fig. 3B). Furthermore, there was no change in abundance, activation and polarization markers, or cytokine expression in both $MHCII^{high}$ or $MHCII^{low}$ macrophages as result of loss of AMPKα1 in CD11c-expressing cells (Supp. Fig. 3C-G). Thus, at population level AMPK signaling only appears to selectively limit CD86 expression by cDC1s in both tumor and TDLNs.

AMPK activation suppresses ACC1 expression and limits accumulation of $GLUT1^{+}$ TA-cDC1s

Given the known role for AMPK in driving metabolic changes (3) and the importance for metabolism in shaping DC immunogenicity (9) and tolerogenicity (20,21), we hypothesized that AMPKα1-deficiency might affect intracellular metabolism, thereby affecting immunogenicity

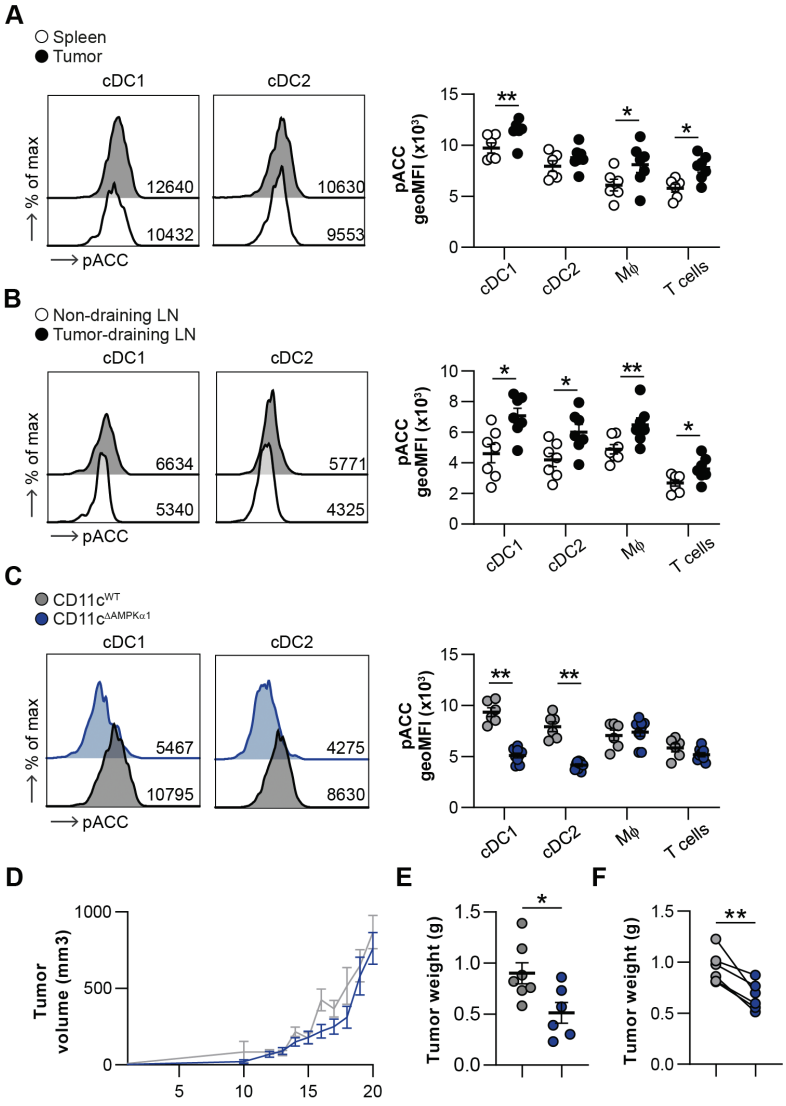

Figure 1: AMPK signaling in TA-DCs promotes tumor growth. A,B: Representative histogram and normalized quantification of phosphorylation levels of ACC (Ser79) (pACC) in cDC1s, cDC2s, macrophages (mφ), and T cells derived from (A) spleen and tumor, (B) non-draining inguinal lymph node and tumor-draining inguinal lymph node. **C:** Representative histogram and normalized quantification of pACC levels in splenic immune cells derived from CD11c^{WT} and CD11c$^{\Delta AMPK\alpha1}$ mice. **D:** B16F10-OVA melanoma growth kinetics in CD11c^{WT} and CD11c$^{\Delta AMPK\alpha1}$ mice. n = 43-46. **E,F:** Mice were sacrificed after approximately 20 days and tumors were weighed. Tumor weight of **(E)** one representative experiment and **(F)** the average tumor weight of individual experiments. Results are expressed as means ± SEM. Statistical analyses were performed using unpaired or paired t-tests, *p < 0.05, **p < 0.01.

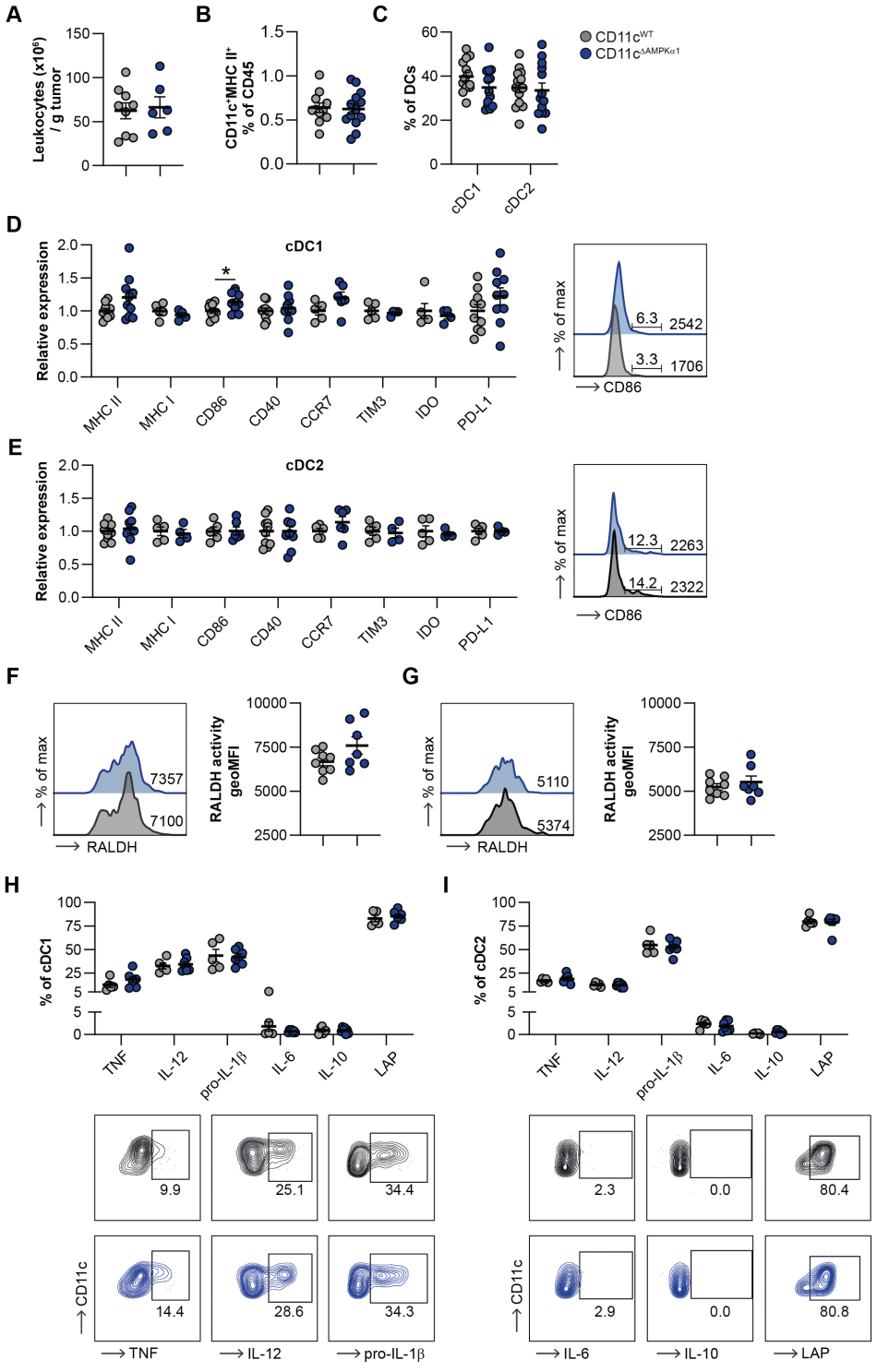
A
Leukocytes (x10⁶) / g tumor
B
CD11c+MHC II+ % of CD45
C
% of DCs
cDC1
cDC2
CD11c^WT
CD11c^ΔAMPKα1
D
cDC1
Relative expression
MHC II
MHC I
CD86
CD40
CCR7
TIM3
IDO
PD-L1
% of max
6.3
2542
3.3
1706
CD86
E
cDC2
12.3
2263
14.2
2322
F
RALDH
7357
7100
RALDH activity geoMFI
G
5110
5374
H
% of cDC1
TNF
IL-12
pro-IL-1β
IL-6
IL-10
LAP
9.9
25.1
34.4
14.4
28.6
34.3
CD11c
I
% of cDC2
2.3
0.0
80.4
2.9
0.0
80.8

Figure 2: Effects of AMPK signaling on TA-DC activation. A: Absolute number of total leukocytes in tumor samples. **B,C:** Frequencies of **(B)** total $CD11c^{+}MHCII^{+}$ DCs and **(C)** of cDC1s and cDC2s. **D,E:** Relative expression of activation markers on tumor-derived **(D)** cDC1s and **(E)** cDC2s and representative histogram of CD86 levels. **F,G:** Representative histogram and quantification of RALDH activity in **(F)** TA-cDC1s and **(G)** TA-cDC2s. **H,I:** Tumor digests were stimulated with LPS and CpG in the presence of Brefeldin A for intracellular cytokine detection. Representative plots and percentages of cytokine expression within **(H)** cDC1s and **(I)** cDC2s. Results are expressed as means ± SEM. Statistical analyses were performed using unpaired t-tests, *$p < 0.05$.

and anti-tumor immunity. Hence, we addressed metabolic rewiring in $CD11c^{\Delta AMPK\alpha1}$ mice and $CD11c^{WT}$ mice using various metabolic dyes (22). No changes in glucose uptake (2-NBDG), long chain fatty acid uptake (Bodipy C16), lipid droplets (LipidTOX), or mitochondrial mass (Mitotracker Deep Red (MDR)) were observed in AMPKα1-deficient TA-DCs and TDLN DCs, but AMPKα1-deficient TDLN cDC1s showed a decrease in mitochondrial membrane potential (TMRM) (Supp. Fig. 4A-D).

To further explore the metabolic consequence of AMPKα1-deficiency in TA-DCs, we analyzed the expression of key metabolic enzymes (Supp. Fig. 4E), as a proxy for activity of core metabolic pathways (23,24). Interestingly, both TA-cDC1s and cDC2s from $CD11c^{\Delta AMPK\alpha1}$ mice showed an increase in acetyl-CoA carboxylase-1 (ACC1) expression, a rate-limiting enzyme in fatty acid synthesis, and a small decrease for glucose-6-phosphate dehydrogenase (G6PD), a key enzyme in the pentose phosphate pathway. AMPKα1-deficient TA-cDC2s additionally had reduced expression of glucose transporter 1 (GLUT1) and enhanced expression of succinate dehydrogenase A (SDHA), a TCA cycle/electron transport chain enzyme (Fig. 3A,B).

As the tumors of $CD11c^{\Delta AMPK\alpha1}$ mice are smaller compared to those of $CD11c^{WT}$ mice, the metabolic changes between $CD11c^{WT}$ and $CD11c^{\Delta AMPK\alpha1}$ TA-DCs can be a consequence of changes in the metabolic tumor micro-environment, instead of, or in addition to, being a result of cell-intrinsic altered AMPK signaling. Hence, we addressed whether $CD11c^{neg}$ cells (Supp. Fig. 4H) (T cells, B cells, monocytes, and neutrophils), that should not be affected by intrinsic AMPKα1-deficiency, also showed differences in expression of metabolic markers when comparing $CD11c^{\Delta AMPK\alpha1}$ mice to $CD11c^{WT}$ mice. Interestingly, most changes observed in TA-DCs, also occurred in tumor-infiltrating T cells, B cells, and monocytes. Neutrophils also showed metabolic differences between $CD11c^{WT}$ and $CD11c^{\Delta AMPK\alpha1}$ mice, but distinct from the other immune cell subsets (Fig. 3C). The metabolic differences observed in tumor-infiltrating $CD11c^{neg}$ leukocytes were absent or reduced in leukocytes derived from lymph nodes or spleen, while most metabolic changes observed in TA-DCs were still present, or even stronger in TDLN and/or NDLN (Fig. 3D-F). Furthermore, a consistent increase in ACC1 for AMPKα1-deficient DCs was observed within all tissues, suggesting that AMPK signaling suppresses expression of metabolic markers, and in particular ACC1, independent of the TME. Downregulation of G6PD and GLUT1 in AMPKα1-deficient TA-DCs, on the other hand, is likely to be a consequence of changes in tumor specific signals between $CD11c^{WT}$ and $CD11c^{\Delta AMPK\alpha1}$ mice, as this was not observed in other tissues, but was visible in TA-$CD11c^{neg}$ immune cells. This indicates that the effect of loss of AMPKα1 on TA-DC metabolism is not only cell intrinsic, but may also be secondary to difference in tumor size as evidenced by overlapping metabolic changes with other TA-immune cells.

To better map potential heterogeneity in metabolic and immunological profiles within TA-DC subsets as a consequence of loss of AMPKα1, we performed an unsupervised clustering

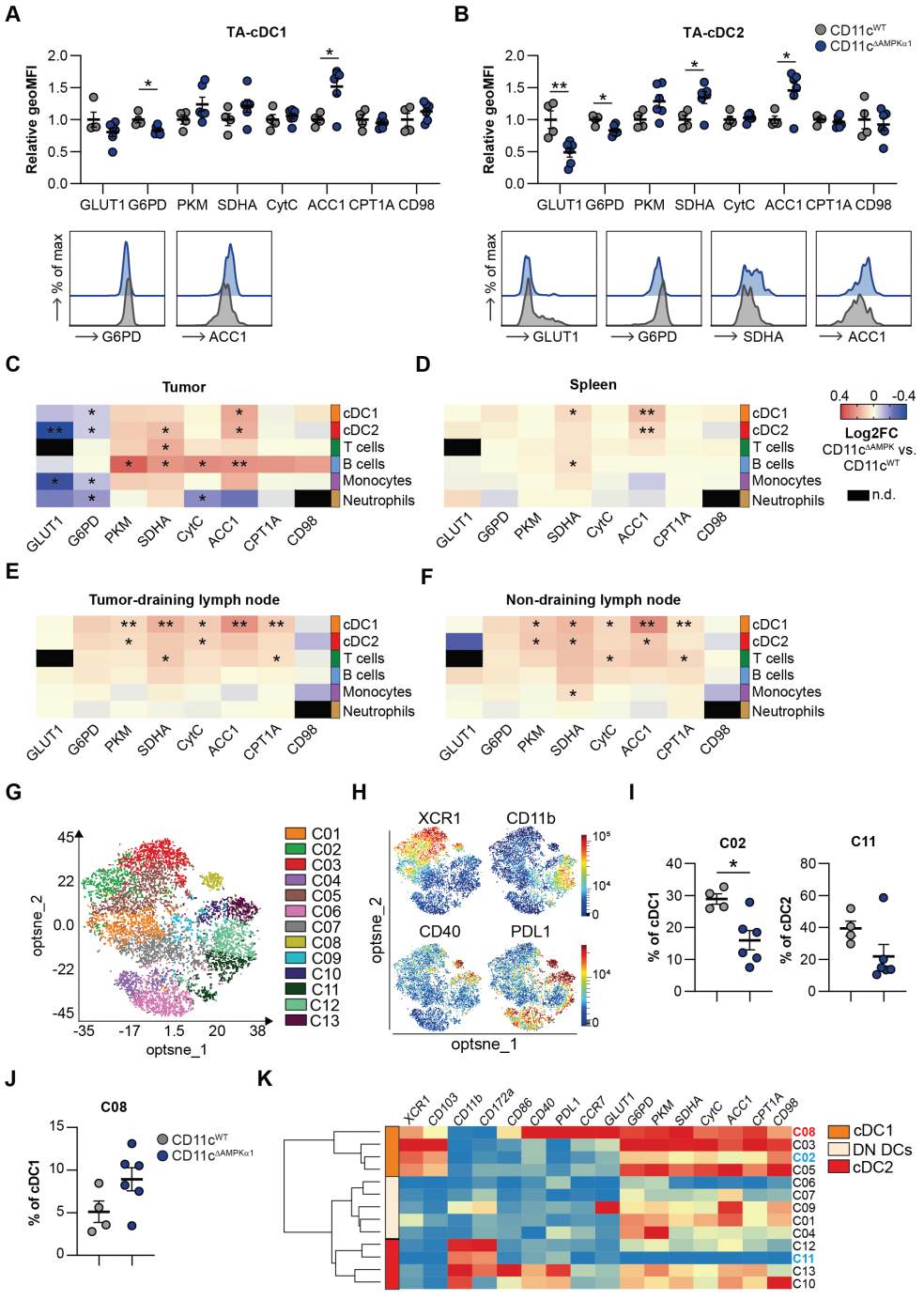
A
TA-cDC1
Relative geoMFI
GLUT1 G6PD PKM SDHA CytC ACC1 CPT1A CD98
% of max
G6PD
ACC1
B
TA-cDC2
CD11c^WT
CD11c^ΔAMPKα1
GLUT1
SDHA
C
Tumor
D
Spleen
Log2FC
CD11c^ΔAMPK vs. CD11c^WT
n.d.
cDC1
cDC2
T cells
B cells
Monocytes
Neutrophils
E
Tumor-draining lymph node
F
Non-draining lymph node
G
optsne_1
optsne_2
C01 C02 C03 C04 C05 C06 C07 C08 C09 C10 C11 C12 C13
H
XCR1
CD11b
CD40
PDL1
I
C02
C11
% of cDC1
% of cDC2
J
C08
K
XCR1 CD103 CD11b CD172a CD86 CD40 PDL1 CCR7 GLUT1 G6PD PKM SDHA CytC ACC1 CPT1A CD98
DN DCs

Figure 3: AMPK signaling induces metabolic changes in TA-DCs. A,B: Relative expression of metabolic markers and representative histograms of tumor-derived **(A)** cDC1s and **(B)** cDC2s. **C-F:** Heatmaps showing relative expression levels of metabolic markers in immune cells isolated from **(C)** tumor, **(D)** spleen, **(E)** TDLN, and **(F)** NDLN, depicted as log2 fold chain (L2FC) from CD11c$^{\Delta AMPK\alpha1}$ when compared to CD11c^{WT} mice. **G:** Clusters derived from FlowSOM clustering performed on tumor-derived CD11c^{+}MHCII^{+} DCs using activation, lineage and metabolic markers. **H:** Expression intensity of XCR1, CD11b, CD40 and PD-L1 on FlowSOM clusters. **I,J:** Most **(I)** downregulated and **(J)** upregulated clusters from CD11c$^{\Delta AMPK\alpha1}$ mice compared to CD11c^{WT} mice depicted as frequencies of parent DC subset. **K:** Heatmap showing mean expression levels in FlowSOM clusters. Double negative DCs (DN DCs). Results are expressed as means ± SEM. Statistical analyses were performed using unpaired t-tests, *p < 0.05, **p < 0.01. n.d. = not detectable.

analysis on CD11c^{+}MHCII^{+} TA-DCs based on lineage, activation, and metabolic markers. This revealed 13 clusters that separated cDC1s, cDC2s, and a DC subset negative for both cDC1 and cDC2 markers (double negative DCs) (Fig. 3G,H). Differential cluster abundance analysis between CD11c^{WT} and CD11c$^{\Delta AMPK\alpha1}$ TA-DCs highlighted changes in frequencies of clusters C08, C02, and C11 (Supp Fig. 4F and Fig. 3I,J). Interestingly, C02 and C11 are subsets of cDC1s and cDC2s respectively, whose abundance decreased in CD11c$^{\Delta AMPK\alpha1}$ mice (Fig. 3I), and are characterized by low expression of metabolic enzymes (Fig. 3K), suggesting that AMPK activation suppresses metabolic activity in particular TA-DC subsets. Furthermore, the abundance of C08 was higher in CD11c$^{\Delta AMPK\alpha1}$ mice and represents a subset of cDC1s with high expression of activation and metabolic markers, in particular GLUT1 (Fig. 3J,K and Supp. Fig. 4G).

Taken together, these data suggest that AMPK signaling in TA-DCs suppresses expression of key metabolic enzymes, in particular ACC1, drives accumulation of cDC1s and cDC2s with low metabolic activity, and prevents accumulation of a GLUT1^{+} cDC1 subset with a high activation status.

ACC activity in CD11c^{+} cells suppresses Treg induction *ex vivo*

The observed increase in ACC1 expression in DCs from CD11c$^{\Delta AMPK\alpha1}$ mice could reflect enhanced fatty acid synthesis (FAS), a metabolic feature linked to increased DC immunogenicity (25). Hence, we hypothesized that AMPK signaling in TA-DCs may limit CD4^{+} and CD8^{+} T cell priming by restricting ACC expression/activity. To test this, we co-cultured tumor-derived OVA-stimulated CD11c^{+} cells from CD11c^{WT} and CD11c$^{\Delta AMPK\alpha1}$ (Supp. Fig. 5A) with naïve CD4^{+} OT-II cells, or naïve CD8^{+} OT-I cells (Fig. 5A). To evaluate the effects of ACC expression in TA-DCs on T cell priming and polarization, we cultured CD11c^{+} cells prior to T cell co-culture in presence or absence of ACC inhibitor CP 640,186 (ACCi), which inhibits both ACC1 and ACC2, thereby inhibiting FAS and promoting FAO, respectively. AMPKα1-deficiency in TA-CD11c^{+} cells did not affect CD4^{+} T cell activation or Treg induction *ex vivo*, as no differences in CD44^{+}, FoxP3^{+}, CTLA-4^{+}, PD-1^{+}, or CD25^{+} populations could be found after 3 days of culturing (Fig. 4B). TNF, IFN-γ, IL-10, and LAP (as a proxy for TGF-β) expression following polyclonal restimulation after 8 days of co-culture were also unaffected by loss of AMPKα1 in TA-CD11c^{+} cells (Supp. Fig. 5B,C). Interestingly, irrespective of the genetic background ACC inhibition in TA-CD11c^{+} cells resulted in decreased CD44, CTLA-4, and PD-1 expression (Fig. 4B,C), and promoted TNF expression by co-cultured CD4^{+} T cells (Supp. Fig. 5A). LAP and Foxp3 expression additionally increased upon ACC inhibition selectively in WT-CD11c^{+}

cells. AMPKα1-deficiency in TA-CD11c$^+$ cells did also not affect CD8$^+$ T cell priming *ex vivo*, indicated by similar proliferation rates, CD44 and PD-1 expression, and no differences in TNF, IFN-γ, and IL-10 expression (Fig. 4D and Supp. Fig. 5D). ACC inhibition in TA-CD11c$^+$ DCs from both CD11c^{WT} and CD11c$^{\Delta AMPK\alpha1}$ mice lowered PD1 expression, while CD44 expression, proliferation rates, and cytokine expression were unaffected (Fig. 4D and Supp. Fig. 5D). Together, these results indicate that ACC expression favors immunogenic CD4$^+$ T cell priming by TA-CD11c$^+$ cells *ex vivo*, irrespective of AMPK signaling.

As AMPK is activated upon nutrient-stress, we hypothesized that the absence of differences in T cell priming capacity between TA-DCs from CD11c^{WT} and CD11c$^{\Delta AMPK\alpha1}$ mice *ex vivo* might be a consequence of exposure to nutrient-rich culture media, a context in which AMPK signaling would be minimal. Therefore, we sorted splenic cDC2s from CD11c^{WT} and CD11c$^{\Delta AMPK\alpha1}$ mice and cultured cells in B16-conditioned medium (B16 CM) or control IMDM, in presence of OVA, after pre-incubation with DMSO or ACCi. After overnight incubation we washed the cells and started a co-culture with naïve CD4$^+$ T cells (Fig. 4F). Of note, a similar protocol was applied for cDC1s, but they did not survive. However, also this experimental setup did not reveal differences in CD4$^+$ T cell priming between TA-cDC2s isolated from CD11c^{WT} and CD11c$^{\Delta AMPK\alpha1}$ mice (Fig. 4G,H and Supp. Fig. 5E). Similar to our previous results, ACC inhibition promoted FoxP3 and dampened CD44, CTLA-4, and PD-1 expression (Fig. 4G,H and Supp. Fig. 5E). Additionally, a decrease in CD25 expression upon ACC inhibition was found (Supp. Fig. 5E). Summarized, *ex vivo* co-culture experiments could not discern a difference in T cell priming potential between AMPKα1-deficient and sufficient TA-DCs, although they do indicate that increased ACC1 expression in AMPKα1-deficient TA-DCs may reduce their ability to prime FoxP3$^+$ Tregs.

AMPK activation in TA-DCs has a limited effect on intra-tumoral T cells

We next aimed to assess to what extent these *ex vivo* T cell priming data by AMPKα1-deficient TA-DCs would be mirrored *in vivo* and whether there are differences in the intra-tumoral T cell compartment that can explain the decrease in tumor growth observed in CD11c$^{\Delta AMPK\alpha1}$ mice when compared to CD11c^{WT} mice. Total T cell abundance and CD4$^+$ or CD8$^+$ frequencies were similar in tumors from CD11c^{WT} and CD11c$^{\Delta AMPK\alpha1}$ mice (Fig. 5A,B). Further assessment of the CD4$^+$ T cell compartment did not reveal differences in the abundance of CD44$^+$CD62L$^-$ effector T cells or FoxP3$^+$ Tregs (Fig. 5C,D). Within the Treg compartment, CTLA-4, PD-1 or KLRG1 expression did not differ between CD11c^{WT} and CD11c$^{\Delta AMPK\alpha1}$ mice (Fig. 5E) and polyclonal restimulation did not show differences in TNF or IFN-γ expression by CD4$^+$ T cells, although an increase in IL-10 expression was observed as a consequence of loss of AMPKα1 in CD11c-expressing cells (Fig. 5F). Likewise, abundance of activated CD44$^+$ CD8$^+$ T cells, PD-1$^+$ or KLRG1$^+$ CD8$^+$ T cells was similar between tumors from CD11c^{WT} and CD11c$^{\Delta AMPK\alpha1}$ mice and also no differences in frequency of OVA-specific CD8$^+$ T cells could be detected (Fig. 5G-I). OVA-specific restimulation and polyclonal restimulation using PMA/ionomycin were used to asses cytokine expression in CD8$^+$ T cells and although IFN-γ and IL-10 levels were similar between both genotypes, expression of TNF was increased upon polyclonal restimulation (Fig. 5J,K). We also investigated expression of LAMP-1 on the membrane, as marker for recent degranulation, as well as the expression of cytotoxic mediators granzyme B (GZB) and perforin, and observed that these were similar between TA-CD8$^+$ T cells from CD11c^{WT} and CD11c$^{\Delta AMPK\alpha1}$ mice (Fig. 5L). Finally, abundance of other major immune cell subsets found in the TME, including B cells and NK cells (Supp. Fig. 6A), as well as activation

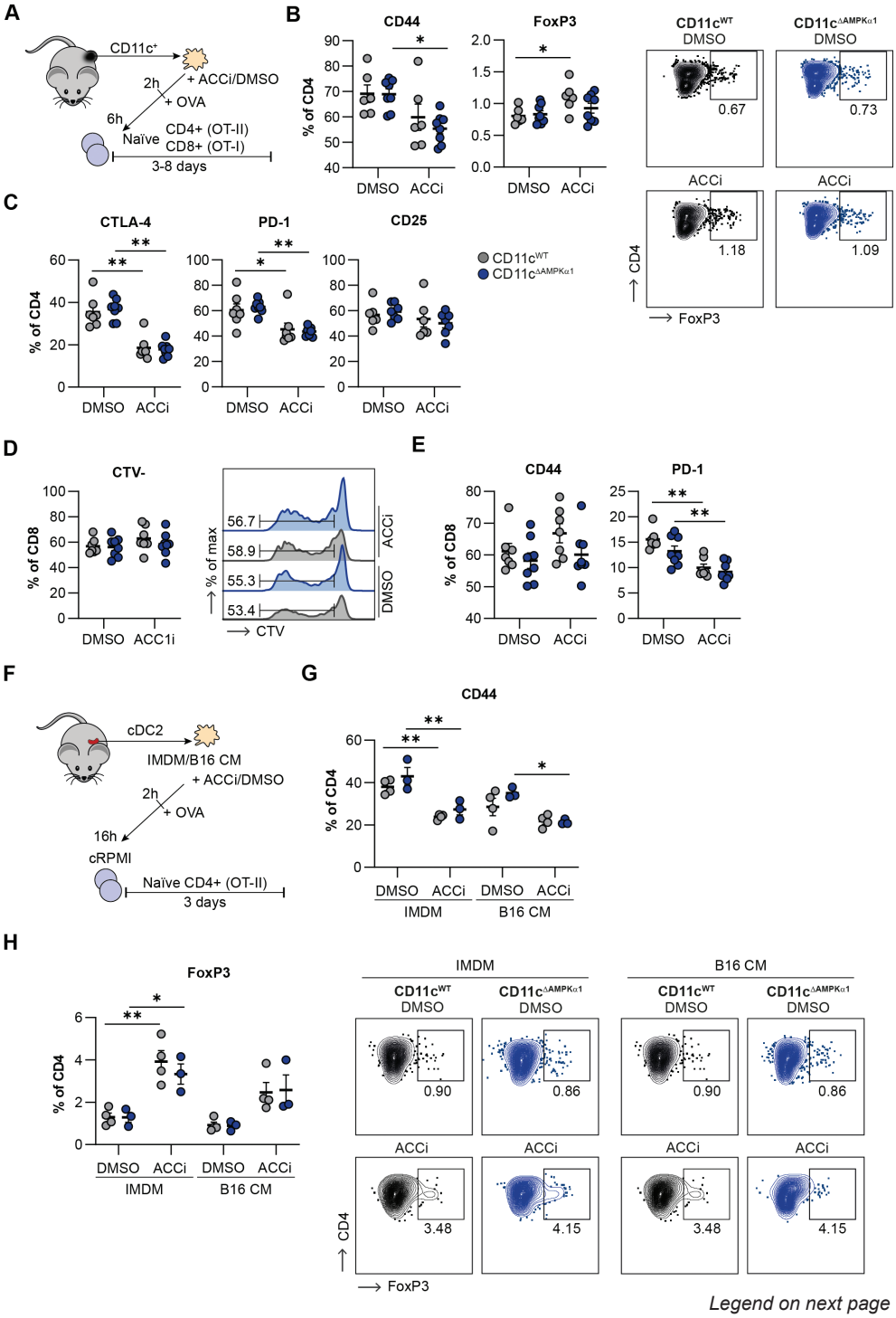

Legend on next page

Figure 4: ACC expression, but not AMPK activation in DCs affects *ex vivo* T cell priming. A: CD11c$^+$ cells were isolated from tumors and cultured in the presence of ACCi or DMSO for 2 hours, before OVA was added. After an additional 4 hours cells were washed and co-cultured with naïve CD4$^+$ OT-II or naïve CD8$^+$ OT-I cells. After 3 days cells were fixed for T cell characterization and proliferation rates, after 8 days cells were used for cytokine analyses. **B,C:** Characterization of CD4$^+$ T cells. (**B**) Frequency of CD44- and FoxP3-expressing cells within total CD4$^+$ T cells and representative plots for FoxP3. (**C**) Frequency of CTLA-4, PD-1, and CD25 expressing cells within total CD4$^+$ T cells. **D,E:** Characterization of CD8$^+$ T cells. (**D**) Proliferation rates and representative histograms and (**E**) percentage of CD44+ and PD-1+ cells within total CD8$^+$ T cells. **F:** cDC2s were sorted from spleens and cultured in IMDM or B16 conditioned medium in the presence of ACCi or DMSO for 2 hours, before OVA was added. After overnight culture cells were washed and co-cultured with naïve CD4$^+$ OT-II T cells. After 3 days cells were fixed for T cell characterization. **G,H:** (**G**) CD44 and (**H**) FoxP3 expression by CD4$^+$ T cells and representative plots for FoxP3 staining. Results are expressed as means ± SEM. Statistical analyses were performed using two-way Anova with Tukey post-hoc test. *$p < 0.05$, **$p < 0.01$.

phenotype of the latter (Supp. Fig. 6B-D), were similar between tumors in both mouse strains. These data suggest that AMPKα1-deficiency in TA-DCs has little impact on CD4$^+$, CD8$^+$, and NK-cell responses in the TME, although we did find AMPK signaling in DCs to suppress TNF secretion by TA-CD8$^+$ T cells.

Discussion

AMPK is a major regulator of cellular metabolism that is activated upon metabolic stress (26) and has anti-inflammatory effects (9,27). This let us to hypothesize that AMPK may serve as a link between nutrient stress and immunosuppression in the TME. Here, we show that AMPK activity is increased in TA-DCs compared to splenic DCs, and similarly TDLN-DCs exhibit higher AMPK signaling compared to NDLN-DCs. Loss of AMPKα1 in DCs leads to a reduction in tumor growth, thereby suggesting that AMPK may limit the capacity of DCs to induce a sufficient anti-tumor immune response. Although it was previously shown that AMPK was required for priming of Tregs by DCs (27), no differences could be found in the Treg-inducing capacity of TA-DCs from CD11c^{WT} and CD11c$^{\Delta AMPK\alpha1}$ mice. However, AMPKα1-deficient cDC1s had increased CD86 expression and tumor-infiltrating CD8$^+$ T cells expressed higher levels of TNF, which might contribute to lower tumor growth in CD11c$^{\Delta AMPK}$ mice. Furthermore, we show that AMPK signaling in DCs induces several metabolic changes, including suppression of ACC1 expression, which can affect the T cell priming capacity of DCs.

Although a consistent smaller tumor size was observed 3 weeks after tumor challenge in CD11c$^{\Delta AMPK\alpha1}$ compared to CD11c^{WT} mice, tumor growth kinetics during those 3 weeks did not significantly differ. Possibly, differences in tumor size between CD11c$^{\Delta AMPK\alpha1}$ and CD11c^{WT} mice may only become apparent during the later stages of tumor growth, because it is only in these settings that intra-tumoral metabolic stress level are sufficiently high to trigger AMPK activation in DCs, to subsequently dampen their immunostimulatory potential.

The TME contains various metabolic cues that could potentially activate AMPK (1,2), including low glucose levels (28), hypoxia (17), lactate (29), and metabolically activated long-chain fatty-acids (30). Canonical AMPK activation is induced by a high AMP/ATP ratio and requires LKB1 (26), which was observed to be increased in TA-DCs (11). This could suggest LKB1-induced canonical AMPK activation in TA-DCs. A recent study showed that in

multiple murine cancer models, myeloid cells, particularly macrophages, are well capable of consuming intra-tumoral glucose and can even outcompete tumor cells for glucose uptake (31), indicating that glucose exposure in the TME is not low enough to serve as trigger for AMPK activation in TA-myeloid cells. However, whether this also holds true for DCs remains to be determined. Moreover, most of their work was performed in MC38 cells, which are less glycolytic than B16F10 melanoma tumor cells used in our studies, making it possible that in our model glucose levels may be actually sufficiently low to contribute to induction of AMPK signaling in DCs (16). To address this, direct genetic modification of key enzymes in glycolysis, analogous to what has been done in a model for sarcoma (32), would be a promising approach to selectively assess the consequences of increased or decreased glucose levels in the TME on AMPK activation in tumor-infiltrating leukocytes.

The observation that AMPK signaling is augmented in both TA-DCs and DCs from the TDLN, could indicate that the enhanced AMPK activation is maintained when DCs migrate from tumor to TDLN. Another possibility is that both the TME and the TDLN contain AMPK-inducing factors. For instance, TDLNs can receive lymphatic drainage from tumors and it has been shown that lactic acid from B16F10 melanomas can transfer to TDLN through tumor-associated lymphatic vessels, thereby lowering the pH in TDLN (33). It is possible that other soluble factors from the TME also drain to the TDLN, thereby affecting AMPK signaling and immune cell activation. Further studies are required to discover the tumor-derived factors that promote AMPK activation in tumor as well as TDLN.

Although we cannot exclude a role for other CD11c-expressing cells in contributing to reduced tumor growth in CD11c$^{\Delta AMPK\alpha1}$ mice, the observations that we did not find any changes in frequency or phenotype of other immune cells that expressed some levels of CD11c, would argue for a key role for DCs in driving the phenotype. Indeed, we found effects of AMPK signaling on activation markers of TA-DCs and TDLN-DCs, in particular suppression of CD86 expression on cDC1s, as well as trends for reduced MHC II, CCR7, and PD-L1 levels on cDC1s CD11c^{WT} compared to CD11c$^{\Delta AMPK\alpha1}$ mice. We also assessed expression of markers associated with tolerogenic DCs, including TIM3 (18), IDO (34), and RALDH activity (19), but did not observe AMPK-dependent regulation. Recently, several studies have highlighted existence of regulatory DC populations that are unique in driving tumor progression (35,36). Whether function or abundance of these mregDCs (mature DCs enriched in immunoregulatory molecules) are affected by AMPK signaling remains to be explored.

Metabolically, there were more profound changes as a result of AMPKα1 loss in TA-DCs. Pyruvate kinase M (PKM), a rate-limiting enzyme of glycolysis, SDHA, and ACC1 were all upregulated in AMPKα1-deficient cDC1s and cDC2s in at least two tissues, indicating that AMPK signaling may limit glycolysis and fatty acid synthesis. Furthermore, cytochrome C (CytC), a protein that transfers electrons between complex III and complex IV of the electron transport chain, and carnitine palmitoyltransferase IA (CPT1A), a mitochondrial fatty acid transporter, were significantly upregulated in cDC1s in both TDLN and NDLN and CytC was also significantly increased in TDLN of CD11c$^{\Delta AMPK\alpha1}$ mice. While AMPK is known to promote catabolic metabolism, these data may suggest that in our model AMPK activation limits overall metabolic activity (26). Moreover, within the tumor, loss of AMPKα1 increased the abundance of a GLUT1-expressing cDC1 subpopulation additionally characterized by high expression of activation markers. As glucose metabolism is highly important for DC activation (9,25), it is tempting to speculate this subset of GLUT1^{+} cDC1s play a critical role in enhancing anti-tumor immunity in CD11c$^{\Delta AMPK\alpha1}$ mice. Furthermore, ACC1 expression increased upon AMPK

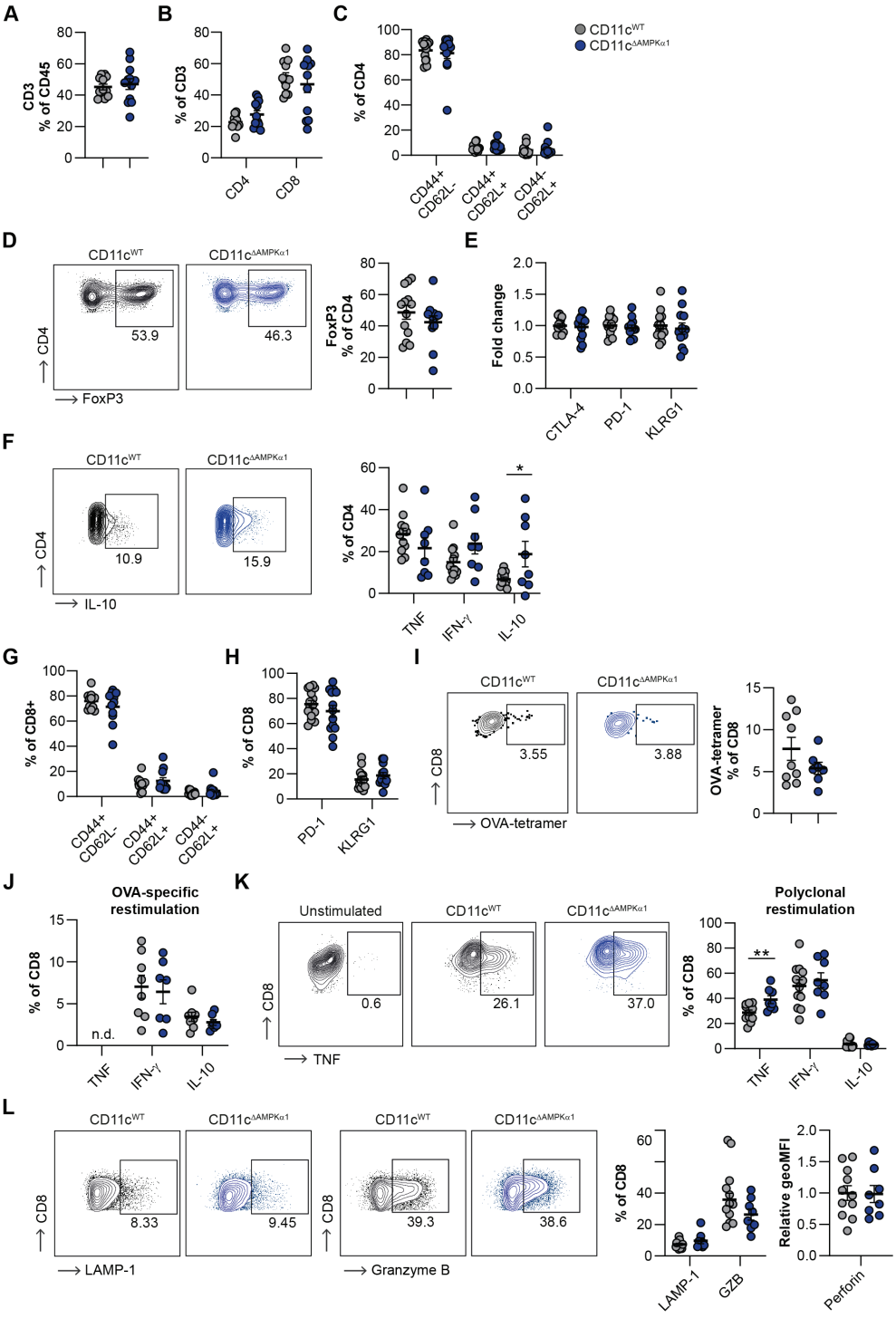
A
B
C
CD3 % of CD45
% of CD3
% of CD4
CD4
CD8
CD44+ CD62L-
CD44+ CD62L+
CD44- CD62L+
CD11c^WT
CD11c^ΔAMPKα1
D
E
F
CD4
FoxP3
53.9
46.3
FoxP3 % of CD4
Fold change
CTLA-4
PD-1
KLRG1
IL-10
10.9
15.9
TNF
IFN-γ
G
H
I
% of CD8+
% of CD8
CD8
OVA-tetramer
3.55
3.88
OVA-tetramer % of CD8
J
K
L
OVA-specific restimulation
Unstimulated
Polyclonal restimulation
n.d.
0.6
26.1
37.0
LAMP-1
Granzyme B
8.33
9.45
39.3
38.6
GZB
Perforin
Relative geoMFI

Figure 5: AMPK signaling DCs limits tumor-infiltrating CD8⁺ T cell activation. A,B: Frequencies of **(A)** total T cells and **(B)** CD4⁺ and CD8⁺ T cells. **C-E:** CD4⁺ T cell characterization. **(C)** Effector vs. naïve T cells frequencies, **(D)** FoxP3⁺ CD4 T cell frequencies and representative plot, and **(E)** expression of levels of CTLA-4, PD-1, and KLRG1 by FoxP3⁺ CD4⁺ T cells. **F:** Cytokine levels after restimulation with PMA and ionomycin in the presence of Brefeldin A and representative plot of IL-10. **G-I:** CD8⁺ T cell characterization. **(G)** Activated and naïve CD8⁺ T cell frequencies, **(H)** expression of PD-1 and KLRG1 on CD8⁺ T cells, and **(I)** representative plots and frequencies of OVA-specific CD8⁺ T cells. **J,K:** Intracellular cytokine staining after **(J)** OVA-specific restimulation and **(K)** PMA and ionomycin restimulation in the presence of Brefeldin A. A representative plot for TNF is shown. **L:** Expression levels and representative plots for cytotoxicity markers. LAMP-1 was added during restimulation with PMA/ionomycin in presence of Brefeldin A and granzyme B and perforin were stained intracellularly. Results are expressed as means ± SEM. Statistical analyses were performed using unpaired t-test. *p < 0.05, **p < 0.01. n.d. = not detectable.

loss in both TA-cDC1s and TA-cDC2s as well as in those DCs from other assessed tissues. It was previously reported that AMPK can transcriptionally repress ACC levels through sterol response element-binding protein 1c (SREBP1c) and hence AMPK activation in TA-DCs may not only inhibit ACC1 activity through phosphorylation (26), but may also limit ACC1 transcription through SREBP1c phosphorylation (37). ACC1 expression is a key enzyme in FAS and it could suggest that AMPK activation suppresses FAS, a metabolic feature known to be important for immunogenic DC activation (25).

Since we previously showed that Treg accumulation during schistosomiasis is reduced in $CD11c^{\Delta AMPK\alpha1}$ compared to $CD11c^{WT}$ mice (27), we hypothesized that the reduced tumor growth could be a consequence of impaired Treg accumulation in the tumors from the KO mice. Furthermore, ACC1 levels increased in AMPKα1-deficient TA-DCs and *ex vivo* data suggest that ACC1 expression in DCs reduces their ability to prime FoxP3⁺ Tregs. However, we did not observe differences in tumor-infiltrating Tregs, nor changes in expression of regulatory markers, between $CD11c^{WT}$ and $CD11c^{\Delta AMPK\alpha1}$ mice. The lack of intra-tumoral Treg differences between $CD11c^{\Delta AMPK}$ and $CD11c^{WT}$ was mirrored by *ex vivo* T cell priming studies with naïve CD4⁺ T cells with tumor-derived CD11c-expressing cells even when *ex vivo* co-cultures with cDC2s activated with OVA in B16 conditioned medium were performed to better mimic the TME *ex vivo*. Hence, TA-DCs do not appear to depend on AMPK activation for Treg priming

On the other hand, we did observe an increase in TNF secretion by CD8⁺ T cells. TNF can have both pro- (38) and anti-tumorigenic (39) functions in B16 melanoma and therefore it remains to be determined whether the increased TNF expression by CD8⁺ T cells contributes to the reduction in tumor growth in $CD11c^{\Delta AMPK\alpha1}$ mice. This enhanced CD8 T cell activation would be largely consistent with our findings that TA-cDC1s from $CD11c^{\Delta AMPK\alpha1}$ displayed a higher activation status . However, *Ex vivo* priming of naïve CD8⁺ T cells did not differ between $CD11c^{\Delta AMPK}$ and $CD11c^{WT}$ cells. This could be related to nutrient-rich culture conditions, or indicate that AMPK signaling in TA-DCs affects their ability to reactivate tumor infiltrating CD8⁺ T cells, rather than CD8⁺ T cell priming itself. In addition to cross-presentation and CD8⁺ T cell activation, TA-cDC1s can also activate and stimulate NK cells (40), but our data did not indicate changes in NK cell function. It is noteworthy that the current study does not include functional T cell assays. *Ex vivo* cytotoxicity assays with tumor-derived CD8⁺ T cells and NK cells, or suppression assays with CD4⁺ T cells may provide new insights into the anti-tumor immune response induced by AMPKα1-deficient TA-DCs.

In summary, in addition to studies in T cells (13) and MDSCs (12), we now show that AMPK signaling in TA-DCs compromises tumor control. Targeting AMPK in TA-DCs could therefore have therapeutic potential. In this context it is important to note that the effect of AMPK blockade in immune cells is not always beneficial for anti-tumor immunity (14) and neither is AMPK inhibition in cancer cells. AMPK can function as a tumor-suppressor by limiting cell growth and proliferation, but also as oncogene by providing protection against metabolic stress caused by poor vascularization (41). Hence, devising strategies for targeted manipulation of AMPK signaling selectively in DCs would be crucial to increase chances of therapeutic success. In addition, it will be interesting to study whether AMPKα1-deficiency in TA-DCs could promote the efficacy of other immunotherapies. For instance, various types of DC vaccines improve PD-L1, CTLA-4 (42) and/or PD-1 blockade (43) in B16F10 melanoma.

Our data indicate that AMPK signaling in TA-DCs and TDLN-DCs promotes tumor growth and inhibits anti-tumor immunity. Although further studies are needed to delineate the exact mechanism that drives tumor progression, AMPK-induced metabolic changes are likely to contribute to altered T cell priming and activation by TA-DCs. Based on our results we propose a role for limited $CD8^+$ T cell activity due to AMPK signaling in DCs, with potentially additional contributions from other T cell populations, that gain immunosuppressive features by AMPK-activated DCs. The recent developments in the field of immunometabolism and the growing interest in targeting metabolism in the TME as therapeutic strategy, make AMPK signaling in TA-DCs a highly relevant topic that warrants further investigations.

Material and methods

Mice

Itgax^{cre} (CD11c) (44), *Prkaa1*$^{fl/fl}$ (AMPKα1) (45) mice, OVA-specific $CD4^+$ T cell receptor transgenic mice (OT-II), and OVA-specific $CD8^+$ T cell receptor transgenic mice (OT-I), all on C57Bl/6J background, were crossed, housed and bred at the LUMC, in a temperature-controlled room with a 12-hour light-dark cycle and *ad libitum* access to food and tap water under specific pathogen free conditions. Experiments were performed in accordance with the Guide for the Care and Use of Laboratory Animals of the Institute for Laboratory Animal Research and have received approval from the Dutch Central Authority for Scientific Procedures on Animals (CCD; animal license numbers AVD116002015253 and AVD1160020186804).

B16F10 culture

B16F10-OVA-expressing melanoma cells were cultured in IMDM (BE12-722F, Lonza), supplemented with 10% heat-inactivated FCS (S-FBS-EU-015, Serana), 100 U/mL penicillin (16128286, Eureco-pharma), 100 µg/mL streptomycin (S9137, Sigma-Aldrich), 1 mg/mL Active Geneticin/G148 (2448984, Gibco), 2 mM L-glutamine (G8540, Sigma-Aldrich), and 1 mM pyruvate (P5280, Sigma-Aldrich). Cells were split two to three times per week.

Tumor challenge

Mice were inoculated subcutaneously with 3×10^5 B16F10-OVA-expressing melanoma cells in 100 µl HBSS without phenol red (14175095, ThermoFisher). Tumor growth was measured three times a week using a caliper and tumor volume was calculated using the ellipsoid volume

formula (1/2 x length x width x height). Mice were euthanized through cervical dislocation after 18-20 days, or when tumor size reached >1500 mm^3 in volume.

Isolation of leukocytes from spleen, inguinal lymph nodes, and tumor

Spleens were collected in 500 µL RPMI 1640 + Glutamax (61870036, Life Technolgies), mechanically disrupted, and digested for 20 min at 37°C in medium supplemented with 1 mg/mL Collagenase D (11088866001, Roche) and 30 U/mL DNase I (D4263, Sigma-Aldrich). Digested samples were filtered through 100 µm filters and subjected to erythrocyte lysis buffer (0.15 M NH_4Cl, 1 mM $KHCO_3$, 0.1 mM Na_2EDTA (15575-038, ThermoFisher) before counting in complete RPMI (cRPMI, RPMI 1640 + Glutamax, supplemented with 10% heat-inactivated FCS, 25 nM β-mercaptoethanol (M6250, Sigma-Aldrich), 100 U/mL penicillin, and 100 µg/mL streptomycin).

Tumors were collected, mechanically disrupted and digested in cRPMI supplemented with 1 mg/mL collagenase type IV from Clostridium histolyticum (C5138, Sigma-Aldrich) and 50 U/mL DNase at 200 rpm for 45 minutes at 37°C. Digested samples were filtered through 100 µm filters and subjected to erythrocyte lysis buffer before counting in cRPMI.

For assessment of *in situ* pACC status of immune cells by flow cytometry (see below), organs were collected and fixed prior to tissue processing in 500 µL of 2% formaldehyde/PBS (220/12257974/1110, Braun), as previously described (22), followed by digestion as described above.

Intracellular cytokine detection

Intracellular cytokine production was analyzed using flow cytometry. For polyclonal restimulation of T cells, tumor-infiltrating leukocytes were restimulated for 4 hours at 37°C in cRPMI with 100ng/mL phorbol myristate acetate (PMA, P8139, Sigma-Aldrich) and 1 ug/mL ionomycin (I0634, Sigma Aldrich) in the presence of 10 µg/mL Brefeldin A (B7651, Sigma-Aldrich) and an anti-CD107a antibody. For OVA-specific restimulation of T cells, tumor-infiltrating leukocytes were co-cultured in cRPMI for 5 hours at 37°C with D1 dendritic cells (46), pre-loaded with 1 µg/mL SIINFEKL, in the presence of Brefeldin A. For *ex vivo* DC and macrophage stimulation, tumor-infiltrating leukocytes were stimulated for 4 hours at 37°C in cRPMI supplemented with 100 ng/mL LPS (0111:B4, InvivoGen) and 5 µg/mL CpG (ODN 1826, InvivoGen) in the presence of Brefeldin A.

Flow cytometry

In general, cells were stained with a viability dye (Zombie NIR™ Fixable Viability Kit, 423106 BioLegend) for 20 minutes at room temperature before fixation with 1.85% formaldehyde (F1635, Sigma) or for 1 hour at 4°C with FoxP3/Transcription factor staining buffer set (00-5523-00, Invitrogen). Metabolic dyes, RALDH activity, tetramer, and T cell proliferation were measured in live cells. Surface proteins were stained for 30 minutes at 4°C in FACS buffer (PBS supplemented with 0.5% BSA (10735086001, Roche) and 2mM EDTA (15575-038, ThermoFisher). For intracellular stainings cells were permeabilized for 20 minutes at 4°C in permeabilization buffer (#00-8333-56 – ThermoFisher), before staining for 30 minutes at 4°C in permeabilization buffer. Prior to staining with phospho-ACC, cells were also permeabilized in 96% methanol (67-56-1, Fisher chemical) for 20 minutes at -20°C. Cells were stained with metabolic dyes as previously described (22). Briefly, cells were cultured at 37°C in PBS, supplemented with 2-NBDG (N13195, ThermoFisher), BODIPY™ FL C16

(D3821, ThermoFisher), LipidTOX (H34476, ThermoFisher), TMRM (T668, ThermoFisher) or MitoTracker™ Deep Red FM (M22426, ThermoFisher) prior to measurement. Aldefluor kit (01700, Stemcell Technologies) was used for assessing RALDH activity, according to manufacturer's protocol. Briefly, cells were stained for 30 minutes at 37°C with 1 µM of Aldefluor reagent dissolved in assay buffer. Cells were kept in assay buffer until measurement. Samples were acquired on Cytek Aurora 3-laser of Cytek Aurora 5-laser spectral flow cytometer and analyzed using FlowJo (Version 10.6, TreeStar). Antibody information is provided in Table 1.

***Ex vivo* T cell co-culture assays**

$CD11c^+$ cells were isolated from digested spleens and tumors using LS columns and CD11c MicroBeads (130-125-835, Miltenyi Biotec) according to the manufacturer's protocol. CD11c+ cells were cultured at 37°C in cRPMI and treated with 60 µM ACC inhibitor CP 640,186 (17691-5, Sanbio) or DMSO (102931, Merck Millipore) for 2 hours, before stimulation with 100 µg/mL OVA (vac-pova-100, InvivoGen). After 4 hours cells were washed and co-cultured with naïve $CD4^+$ or $CD8^+$ T cells.

cDC2s were sorted from splenic $CD11c^+$ cells, isolated as described above, and FACS sorted ($MHCII^+$ $CD11c^+$ $CD64^-$ $F4/80^-$ $CD172a^+$ $XCR1^-$) on a BD FACSAria using a 100 µm nozzle at 20 PSI. cDC2s were cultured in B16-conditioned medium (supernatant derived from a one week B16F10 melanoma culture) or control IMDM medium and treated with 60 µM DMSO or ACCi for 2 hours, before stimulation with 100 µg/mL OVA. The next day cells were washed and cultured with naïve $CD4^+$ T cells. Naïve $CD4^+$ T cells and naïve $CD8^+$ T cells were negatively isolated using mojosort mouse CD4/CD8 naïve T cell isolation kits (480040, 480044, BioLegend) from OT-II and OT-I mice, respectively, according to the manufacturer's protocol. $CD8^+$ T cells were stained with Cell Trace Violet (C34557, ThermoFisher) prior to co-culture. 7000 $CD11c^+$ cells were co-cultured with 70,000 T cells and after 3 days half of the cells were harvested to measure proliferation and FoxP3 expression. Remaining cells were supplemented with IL-2 (202-IL, R&D Systems) and used for polyclonal T cell restimulation on day 8.

OMIQ analysis

$CD45^+CD3^-CD19^-SiglecH^-SiglecF^-Ly6C^-Ly6G^-F4/80^-CD64^-CD326^-CD11c^+MHCII^+$ TA-DCs were gated in FlowJo, exported, and uploaded into OMIQ. Samples were subsampled using a maximum equal distribution. After sub-sampling, opt-SNE was performed using activation (CD86, CD80, CD40, CCR7), lineage (XCR1, CD103, CD11b, CD172a), and metabolic markers (GLUT1, G6PD, PKM, SDHA, CytC, ACC1, CPT1A, CD36) using the default settings, followed by FlowSOM clustering using the default settings. EdgeR was used to determine significantly different clusters and the heatmap was generated with Euclidean clustering.

Statistical analysis

Results are expressed as mean ± standard error mean (SEM) except stated otherwise. Data was analyzed using GraphPad Prism (La Jolla, CA, USA). Comparisons between two or more independent data groups were made by Student's T test (parametric data)/ Wilcoxon test (nonparametric data) or analysis of variance test (ANOVA), respectively. $P<0.05$ was considered statistically significant.

Table 1: Antibodies for flow cytometry

Target	Fluorophore	Clone	company	identifier
ACC1	-	EPR23235-147	Abcam	ab269273
B220	BV510	RA3-6B2	BioLegend	103248
CCR7/ CD197	BV786	4B12	BD Bioscience	564355
CD103	BUV661	M290	BD Bioscience	741504
CD107a	BV421	1D4B	Biolegend	121617
CD11b	BUV563	M1/70	BD Bioscience	741242
CD11c	BUV496	HL3	BD Bioscience	750483
CD172a	BUV805	P84	BD Bioscience	741997
CD19	ef450	eBio1D3	eBioscience	48-0193-82
CD206	BV785	C068C2	BioLegend	141729
CD25	PEcy5	PC61.5	BioLegend	102010
CD27	BV605	LG.3A10	BioLegend	124249
CD3	ef450	17A2	eBioscience	48-0032-82
CD3	BV750	17A2	BioLegend	100249
CD326	BV605	G8.8	Biolegend	118227
CD4	PE	RM4-5	eBioscience	12-0042-83
CD4	BV650	GK1.5	BD Bioscience	563232
CD40	BV510	3/23	BD Bioscience	745041
CD44	BUV737	IM7	BD Bioscience	612799
CD44	PEcy7	IM7	eBioscience	25-0441-81
CD45	APC/Fire 810	30-F11	BioLegend	103173
CD45	BUV805	30-F11	BD Bioscience	748370
CD62L	APC/Fire 810	30-F11	BioLegend	103173
CD64	PEdazzle594	X54-5/7.1	BioLegend	139320
CD8	BV711	53-6.7	Biolegend	100759
CD86	AF700	GL-1	BD Bioscience	560581
CD98	BUV615	H202-141	BD Bioscience	752360
CLTA4	BV421	UC10-4B9	BioLegend	106312
F4/80	BV711	BM8	Biolegend	123147
FoxP3	APC	FJK-16s	Invitrogen/ eBioscience	12-5773-82
Goat anti-Rabbit	AF647	-	Invitrogen	A21244
Granzyme B	PE	NGZB	eBio	12-8898-80

IDO	PE	eyedio	eBioscience	12-9477-41
IL-10	AF488	JESS-16E3	Invitrogen	53-7101-82
IL-12	APC	C15.6	BD	554480
IL-6	ef450	MP5-20F3	eBioscience	48-7061-82
KLRG1	Pedazzle	MAFA	Biolegend	138423
LAP	PerCPef710	Tw7-16B4	Invitrogen/ eBioscience	46-9821-82
Ly6C	PerCP-Cy5.5	HK1.4	BioLegend	128011
Ly6G	SB550	1A8	BioLegend	127663
MHC I	PEcy7	AF6-88.5	BioLegend	116519
MHC II	BUV395	2G9	BD Bioscience	743876
NK1.1	PerCP-Cy5.5	PK136	Biolegend	108727
PD-1	BV785	29f.1a12	Biolegend	135225
PD-L1	BUV737	M1H5	BD Bioscience	568825
Perforin	FITC	eBioOMAK-D	eBio	11-9392-80
Phospho-ACC (ser79)	-	D7D11	Cell signaling	11818S
pro-IL1b	PE	NJTEN3	eBioscience	12-7114
Siglec F	BV480	E50-24440	BD Bioscience	
Siglec H	BV750	511	BioLegend	129611
TIM3	FITC	RMT3-23	eBioscience	11-5870-82
TNFa	PE/Cy7	MP6-XT22	BioLegend	506324
XCR1	BV650	ZET	BioLegend	148220
G6PD	-	EPR20668	Abcam	ab210702
CPT1A	-	EPR21843-71-2F	Abcam	ab234111
CytC	-	7H8.2C12	Abcam	ab13575
GLUT1	-	EPR3915	Abcam	ab115730
SDHA	-	EPR9043(B)	Abcam	ab137040
PKM	-	EPR10138(B)	Abcam	ab150377

Acknowledgements

D1 dendritic cells were kindly provided by Marcel Camps and Ferry Ossendorp (LUMC). A special thanks to Marion König and Roos van Schuijlenburg for their help during experiments. This work was supported by an LUMC fellowship awarded to B.E.

References

1. Chang CH, Qiu J, O'Sullivan D, Buck MD, Noguchi T, Curtis JD, et al. Metabolic Competition in the Tumor Microenvironment Is a Driver of Cancer Progression. Cell. 2015;162(6):1229–41.
2. Arner EN, Rathmell JC. Metabolic programming and immune suppression in the tumor microenvironment. Cancer Cell. 2023;41(3):421–33.
3. Hardie DG, Ross FA, Hawley SA. AMPK: A nutrient and energy sensor that maintains energy homeostasis. Nat Rev Mol Cell Biol. 2012;13(4):251–62.
4. Salminen A, Hyttinen JMT, Kaarniranta K. AMP-activated protein kinase inhibits NF-κB signaling and inflammation: Impact on healthspan and lifespan. J Mol Med. 2011;89(7):667–76.
5. Böttcher JP, Reis e Sousa C. The Role of Type 1 Conventional Dendritic Cells in Cancer Immunity. Trends Cancer. 2018;4(11):784–92.
6. Wculek SK, Cueto FJ, Mujal AM, Melero I, Krummel MF, Sancho D. Dendritic cells in cancer immunology and immunotherapy. Nat Rev Immunol. 2020;20(1):7–24.
7. Filin IY, Kitaeva K V., Rutland CS, Rizvanov AA, Solovyeva V V. Recent Advances in Experimental Dendritic Cell Vaccines for Cancer. Front Oncol. 2021;11.
8. Kvedaraite E, Ginhoux F. Human dendritic cells in cancer. Sci Immunol. 2022;7:9409.
9. Krawczyk CM, Holowka T, Sun J, Blagih J, Amiel E, DeBerardinis RJ, et al. Toll-like receptor-induced changes in glycolytic metabolism regulate dendritic cell activation. Blood. 2010;115(23):4742–9.
10. Carroll KC, Viollet B, Suttles J. AMPKα1 deficiency amplifies proinflammatory myeloid APC activity and CD40 signaling. J Leukoc Biol. 2013;94(6):1113–21.
11. Wang Y, Du X, Wei J, Long L, Tan H, Guy C, et al. LKB1 orchestrates dendritic cell metabolic quiescence and anti-tumor immunity. Cell Res. 2019;29(5):391–405.
12. Trillo-Tinoco J, Sierra RA, Mohamed E, Cao Y, de Mingo-Pulido A, Gilvary DL, et al. AMPK alpha-1 intrinsically regulates the function and differentiation of tumor myeloid-derived suppressor cells. Cancer Res. 2019;79(19):5034–47.
13. An J, Ding Y, Yu C, Li J, You S, Liu Z, et al. AMP-activated protein kinase alpha1 promotes tumor development via FOXP3 elevation in tumor-infiltrating Treg cells. iScience. 2022;25(1).
14. Pokhrel RH, Acharya S, Ahn JH, Gu Y, Pandit M, Kim JO, et al. AMPK promotes antitumor immunity by downregulating PD-1 in regulatory T cells via the HMGCR/p38 signaling pathway. Mol Cancer. 2021;20(1).
15. Rao E, Zhang Y, Zhu G, Hao J, Persson XMT, Egilmez NK, et al. Deficiency of AMPK in CD8 + T cells suppresses their anti-tumor function by inducing protein phosphatase-mediated cell death. Oncotarget. 2015;6(10):7944–58.
16. Bohn T, Rapp S, Luther N, Klein M, Bruehl TJ, Kojima N, et al. Tumor immunoevasion via acidosis-dependent induction of regulatory tumor-associated macrophages. Nat Immunol. 2018;19(12):1319–29.
17. Steinberg GR, Hardie DG. New insights into activation and function of the AMPK. Nat Rev Mol Cell Biol. 2022;24:255–72.
18. Dixon KO, Tabaka M, Schramm MA, Xiao S, Tang R, Dionne D, et al. TIM-3 restrains anti-tumour immunity by regulating inflammasome activation. Nature. 2021;595(7865):101–6.
19. Coombes JL, Siddiqui KRR, Arancibia-Cárcamo C V., Hall J, Sun CM, Belkaid Y, et al. A functionally specialized population of mucosal CD103+ DCs induces Foxp3+ regulatory T cells via a TGF-β -and retinoic acid-dependent mechanism. Journal of Experimental Medicine. 2007;204(8):1757–64.
20. Malinarich F, Duan K, Hamid RA, Bijin A, Lin WX, Poidinger M, et al. High Mitochondrial Respiration and Glycolytic Capacity Represent a Metabolic Phenotype of Human Tolerogenic Dendritic Cells. The Journal of Immunology. 2015;194(11):5174–86.

21. Ferreira GB, Vanherwegen AS, Eelen G, Gutiérrez ACF, VanLommel L, Marchal K, et al. Vitamin D3 induces tolerance in human dendritic cells by activation of intracellular metabolic pathways. Cell Rep. 2015;10(5):711–25.
22. Brombacher EC, Patente TA, Quik M, Everts B. Characterization of Dendritic Cell Metabolism by Flow Cytometry. In: Sisirak V, editor. Dendritic Cells Methods in Molecular Biology. 2023. p. 219–37.
23. Pelgrom LR, Patente TA, Otto F, Nouwen L V., Ozir-Fazalalikhan A, van der Ham AJ, et al. mTORC1 signaling in antigen-presenting cells of the skin restrains CD8+ T cell priming. Cell Rep. 2022;40(1):1–17.
24. Heieis GA, Patente TA, Tak T, Almeida L, Everts B. Spectral flow cytometry reveals metabolic heterogeneity in tissue macrophages. BioRxiv. 2022;
25. Everts B, Amiel E, Huang SCC, Smith AM, Chang CH, Lam WY, et al. TLR-driven early glycolytic reprogramming via the kinases TBK1-IKKε supports the anabolic demands of dendritic cell activation. Nat Immunol. 2014;15(4):323–32.
26. Hardie DG, Schaffer BE, Brunet A. AMPK: An Energy-Sensing Pathway with Multiple Inputs and Outputs. Vol. 26, Trends in Cell Biology. 2016. p. 190–201.
27. Patente TA, Brombacher EC, Heieis GA, Pelgrom LR, Zawistowska-Deniziak A, Otto F, et al. Metabolic sensor AMPK licenses CD103+ dendritic cells to induce Treg responses. bioRxiv. 2023;
28. Zhang CS, Hawley SA, Zong Y, Li M, Wang Z, Gray A, et al. Fructose-1,6-bisphosphate and aldolase mediate glucose sensing by AMPK. Nature. 2017;548(7665):112–6.
29. Zhou Y, Liu X, Huang C, Lin D. Lactate Activates AMPK Remodeling of the Cellular Metabolic Profile and Promotes the Proliferation and Differentiation of C2C12 Myoblasts. Int J Mol Sci. 2022;23(22):1–16.
30. Pinkosky SL, Scott JW, Desjardins EM, Smith BK, Day EA, Ford RJ, et al. Long-chain fatty acyl-CoA esters regulate metabolism via allosteric control of AMPK β1 isoforms. Nat Metab. 2020;2(9):873–81.
31. Reinfeld BI, Madden MZ, Wolf MM, Chytil A, Bader JE, Patterson AR, et al. Cell-programmed nutrient partitioning in the tumour microenvironment. Nature. 2021;593(7858):282–8.
32. Chang CH, Qiu J, O'Sullivan D, Buck MD, Noguchi T, Curtis JD, et al. Metabolic Competition in the Tumor Microenvironment Is a Driver of Cancer Progression. Cell. 2015;162(6):1229–41.
33. Riedel A, Helal M, Pedro L, Swietlik JJ, Shorthouse D, Schmitz W, et al. Tumor-Derived Lactic Acid Modulates Activation and Metabolic Status of Draining Lymph Node Stroma. Cancer Immunol Res. 2022;10(4):482–97.
34. Zhao F, Xiao C, Evans KS, Theivanthiran T, DeVito N, Holtzhausen A, et al. Paracrine Wnt5a-β-Catenin Signaling Triggers a Metabolic Program that Drives Dendritic Cell Tolerization. Immunity. 2018;48(1):147–60.
35. Maier B, Leader AM, Chen ST, Tung N, Chang C, LeBerichel J, et al. A conserved dendritic-cell regulatory program limits antitumour immunity. Nature. 2020;580(7802):257–62.
36. Zhang Q, He Y, Luo N, Patel SJ, Han Y, Gao R, et al. Landscape and Dynamics of Single Immune Cells in Hepatocellular Carcinoma. Cell. 2019;179(4):829–45.
37. Li Y, Xu S, Mihaylova MM, Zheng B, Hou X, Jiang B, et al. AMPK phosphorylates and inhibits SREBP activity to attenuate hepatic steatosis and atherosclerosis in diet-induced insulin-resistant mice. Cell Metab. 2011;13(4):376–88.
38. Rodriguez YI, Campos LE, Castro MG, Bannoud N, Blidner AG, Filippa VP, et al. Tumor Necrosis Factor Receptor-1 (p55) Deficiency Attenuates Tumor Growth and Intratumoral Angiogenesis and Stimulates CD8+ T Cell Function in Melanoma. Cells. 2020;9(11).
39. Dondossola E, Dobroff AS, Marchiò S, Cardó-Vila M, Hosoya H, Libutti SK, et al. Self-targeting of TNF-releasing cancer cells in preclinical models of primary and metastatic tumors. Proc Natl Acad Sci U S A. 2016;113(8):2223–8.

40. Bödder J, Zahan T, van Slooten R, Schreibelt G, de Vries IJM, Flórez-Grau G. Harnessing the cDC1-NK Cross-Talk in the Tumor Microenvironment to Battle Cancer. Front Immunol. 2021;11.

41. Vara-Ciruelos D, Russell FM, Grahame Hardie D. The strange case of AMPK and cancer: Dr Jekyll or Mr Hyde? Open Biol. 2019;9(7).

42. Zheng F, Dang J, Zhang H, Xu F, Ba D, Zhang B, et al. Cancer Stem Cell Vaccination With PD-L1 and CTLA-4 Blockades Enhances the Eradication of Melanoma Stem Cells in a Mouse Tumor Model. Journal of Immunotherapy. 2018;41(8):361–8.

43. Yazdani M, Gholizadeh Z, Nikpoor AR, Mohamadian Roshan N, Jaafari MR, Badiee A. Ex vivo dendritic cell-based (DC) vaccine pulsed with a low dose of liposomal antigen and CpG-ODN improved PD-1 blockade immunotherapy. Sci Rep. 2021;11(1).

44. Caton ML, Smith-Raska MR, Reizis B. Notch-RBP-J signaling controls the homeostasis of CD8- dendritic cells in the spleen. Journal of Experimental Medicine. 2007;204(7):1653–64.

45. Nakada D, Saunders TL, Morrison SJ. Lkb1 regulates cell cycle and energy metabolism in haematopoietic stem cells. Nature. 2010;468(7324):653–8.

46. Winzler C, Rovere P, Rescigno M, Granucci F, Penna G, Adorini L, et al. Maturation Stages of Mouse Dendritic Cells in Growth Factor-dependent Long-Term Cultures. Vol. 185, J. Exp. Med. 1997.

Supplementary figures

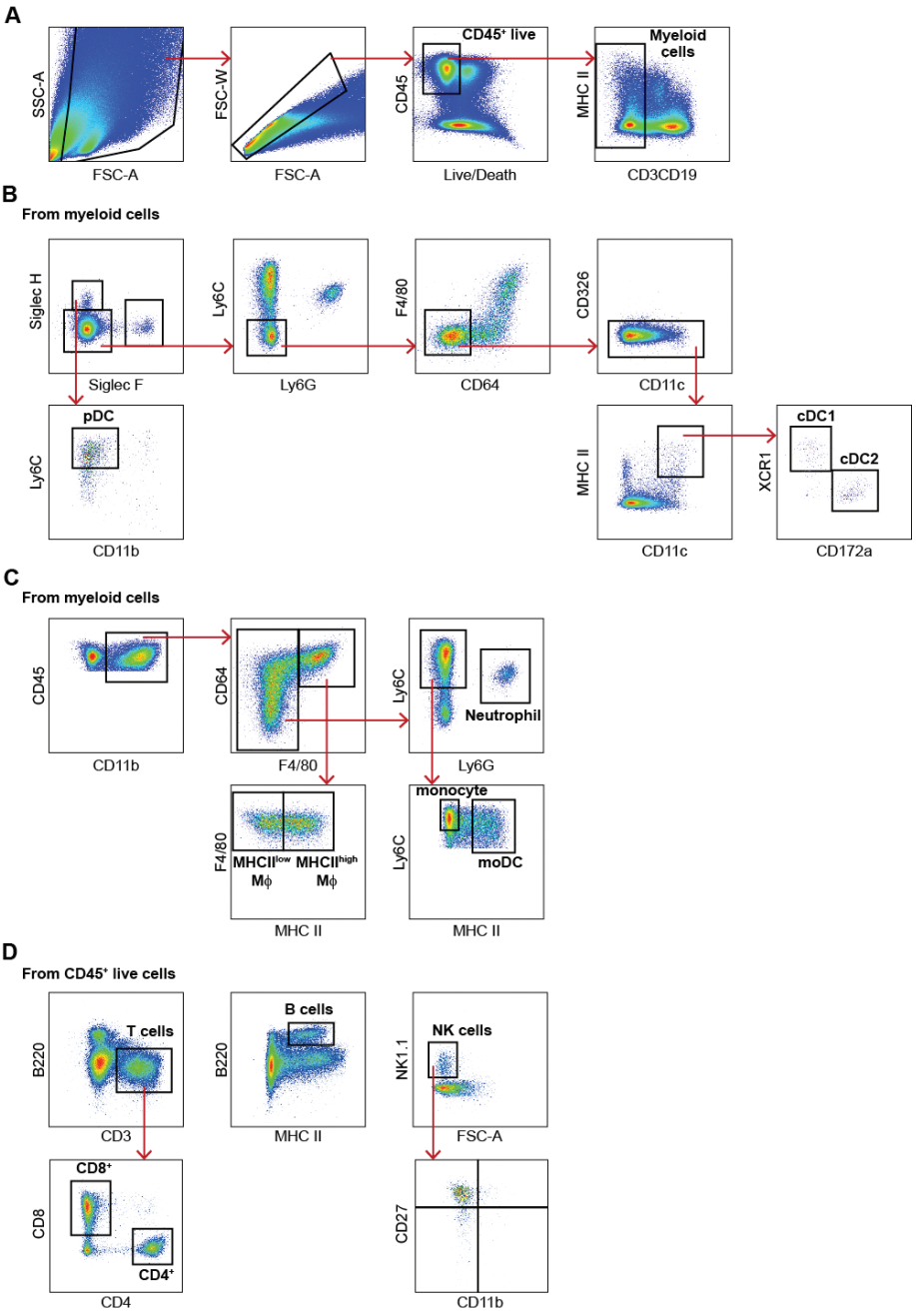

Supplementary figure 1: Gating strategy. A-D: Gating strategy of (A) total myeloid cells from digested tumor samples, **(B)** plasmacytoid DCs (pDCs), cDC1s, and cDC2s, **(C)** neutrophils, macrophages, monocytes, and monocyte-derived DCs (moDCs), and **(D)** T cells, B cells, and NK cells.

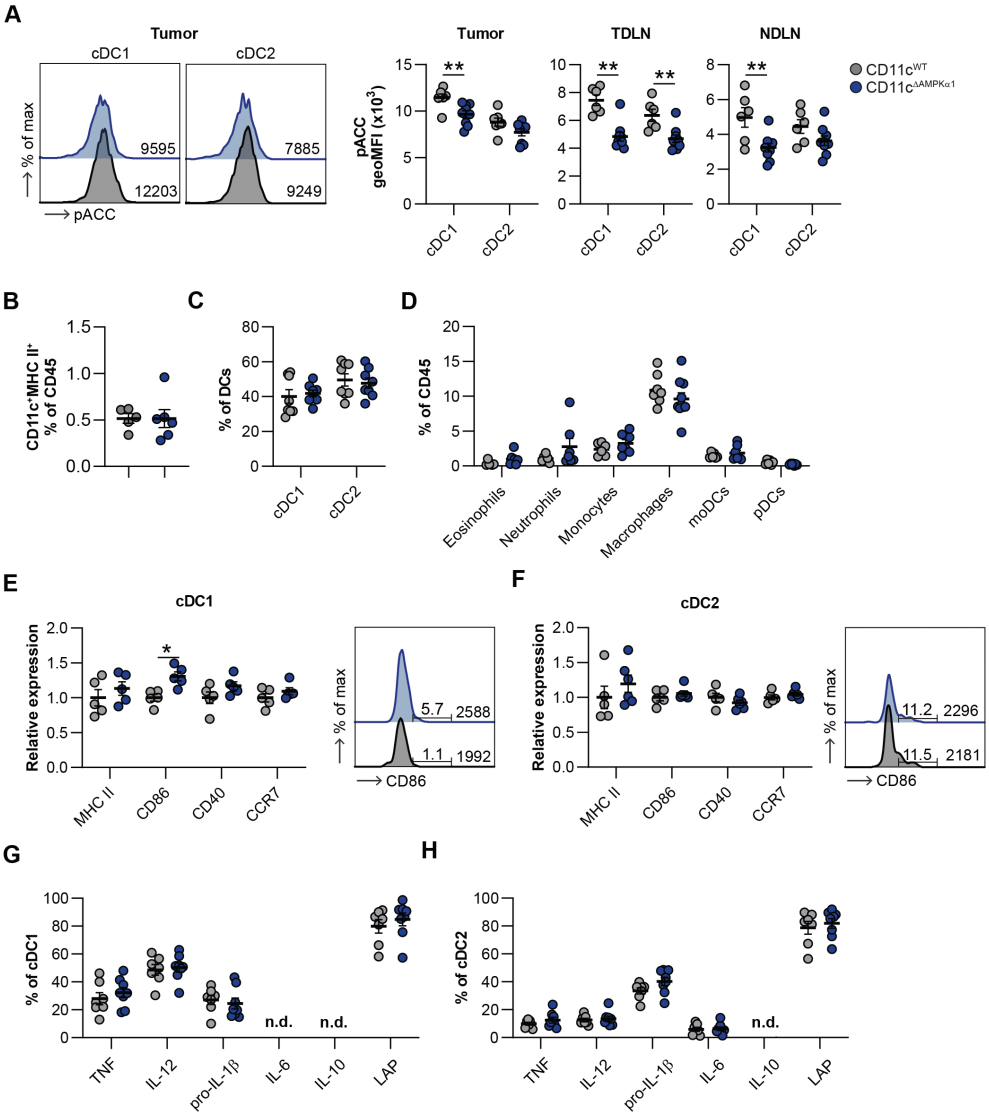

Supplementary figure 2: Effects of AMPK signaling on TDLN-DC activation. A: Representative histogram and normalized quantification pACC levels in cDC1s and cDC2s from tumor, TDLN and NDLN. **B,C:** Frequencies of **(B)** total CD11c⁺MHCII⁺ DCs and **(C)** of cDC1s and cDC2s from TDLN. **D:** Frequencies of myeloid cells in total CD45⁺ live cells derived from tumor samples. **E,F:** Relative expression of activation markers on TDLN-derived **(E)** cDC1s and **(F)** cDC2s and representative histogram of CD86 levels. **G,H:** TDLN digests were stimulated with LPS and CpG in the presence of Brefeldin A for intracellular cytokine detection. Frequencies of cytokine expression within **(G)** cDC1s and **(H)** cDC2s. Results are expressed as means ± SEM. Statistical analyses were performed using unpaired t-tests, *p < 0.05, **p < 0.01. n.d. = not detectable.

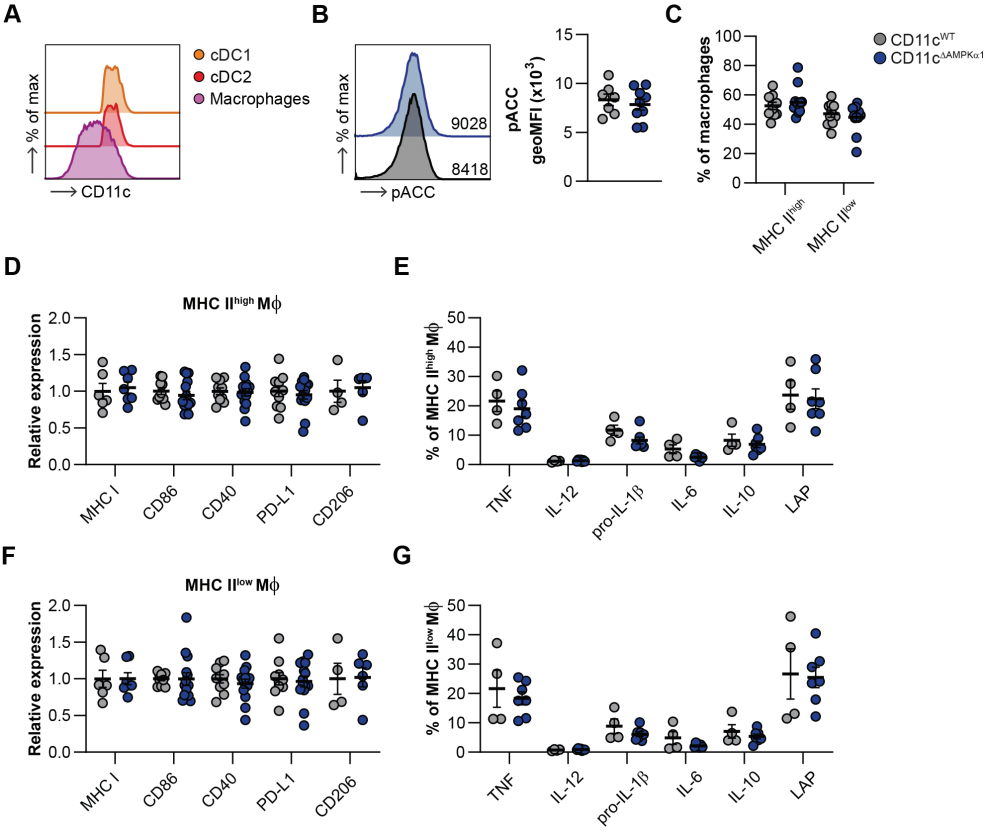

Supplementary figure 3: Macrophage characterization in tumors from CD11c^{WT} and CD11c$^{\Delta AMPK\alpha1}$ mice. A: Representative histogram of CD11c levels in tumor-derived cDC1s, cDC2s, and macrophages **B:** Representative histogram and normalized quantification pACC in macrophages. **C:** Frequencies of MHCII^{low} and MHCII^{high} macrophages. **D-G:** Relative expression of activation markers after tumor digestion, and cytokine levels after LPS + CpG stimulation in presence of Brefeldin A in **(D,E)** MHCII^{high} macrophages and **(F,G)** MHCII^{low} macrophages. Results are expressed as means ± SEM. Statistical analyses were performed using unpaired t-tests, *p < 0.05, **p < 0.01. n.d. = not detectable.

Supplementary figure 4: AMPKα1-deficiency affects metabolism of DCs. A-D: Relative expression and representative histograms of metabolic dyes in tumor-derived **(A)** cDC1s and **(B)** cDC2s, and TDLN-derived **(C)** cDC1s and **(D)** cDC2s. **E:** Illustration indicating metabolic targets and associated metabolic pathways that were assessed using flow cytometry. GLUT1 = Glucose transporter 1. G6PD = Glucose-6-phosphate dehydrogenase, PKM = Pyruvate kinase M, SDHA = Succinate Dehydrogenase A, CytC = Cytochrome C, ACC1 = Acetyl-CoA carboxylase 1, CPT1a = Carnitine Palmitoyltransferase 1A. **F:** Volcano plot of differential expression analysis between flowsom clusters from TA-DCs from CD11c^{WT} and CD11c$^{\Delta AMPK\alpha1}$ mice. **G:** Manual gating confirms high GLUT1 expression in CD86^{+}CD40^{+} cDC1s. **H:** Representative histogram of CD11c expression in tumor-derived immune cells. Results are expressed as means ± SEM. Statistical analyses were performed using unpaired t-tests (**A-D**), *p < 0.05.

Figure on next page

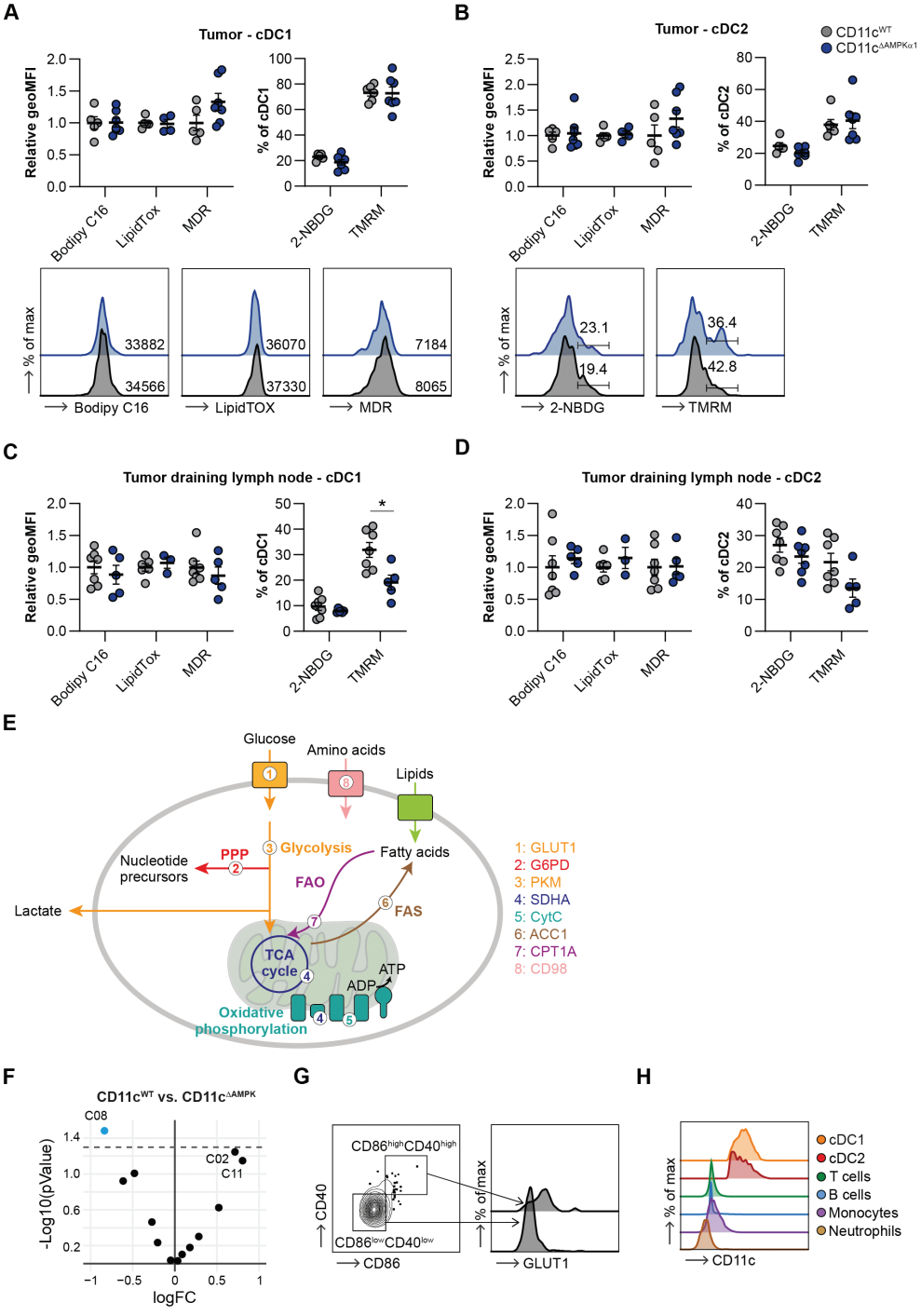
A
Tumor - cDC1
Relative geoMFI
% of cDC1
Bodipy C16
LipidTox
MDR
2-NBDG
TMRM
% of max
33882
34566
36070
37330
7184
8065
B
Tumor - cDC2
CD11c^WT
CD11c^ΔAMPKα1
% of cDC2
23.1
19.4
36.4
42.8
C
Tumor draining lymph node - cDC1
D
Tumor draining lymph node - cDC2
E
Glucose
Amino acids
Lipids
Nucleotide precursors
PPP
Glycolysis
Fatty acids
FAO
FAS
Lactate
TCA cycle
ATP
ADP
Oxidative phosphorylation
1: GLUT1
2: G6PD
3: PKM
4: SDHA
5: CytC
6: ACC1
7: CPT1A
8: CD98
F
CD11c^WT vs. CD11c^ΔAMPK
-Log10(pValue)
logFC
C08
C02
C11
G
CD86^high CD40^high
CD86^low CD40^low
CD40
CD86
GLUT1
H
cDC1
cDC2
T cells
B cells
Monocytes
Neutrophils
CD11c

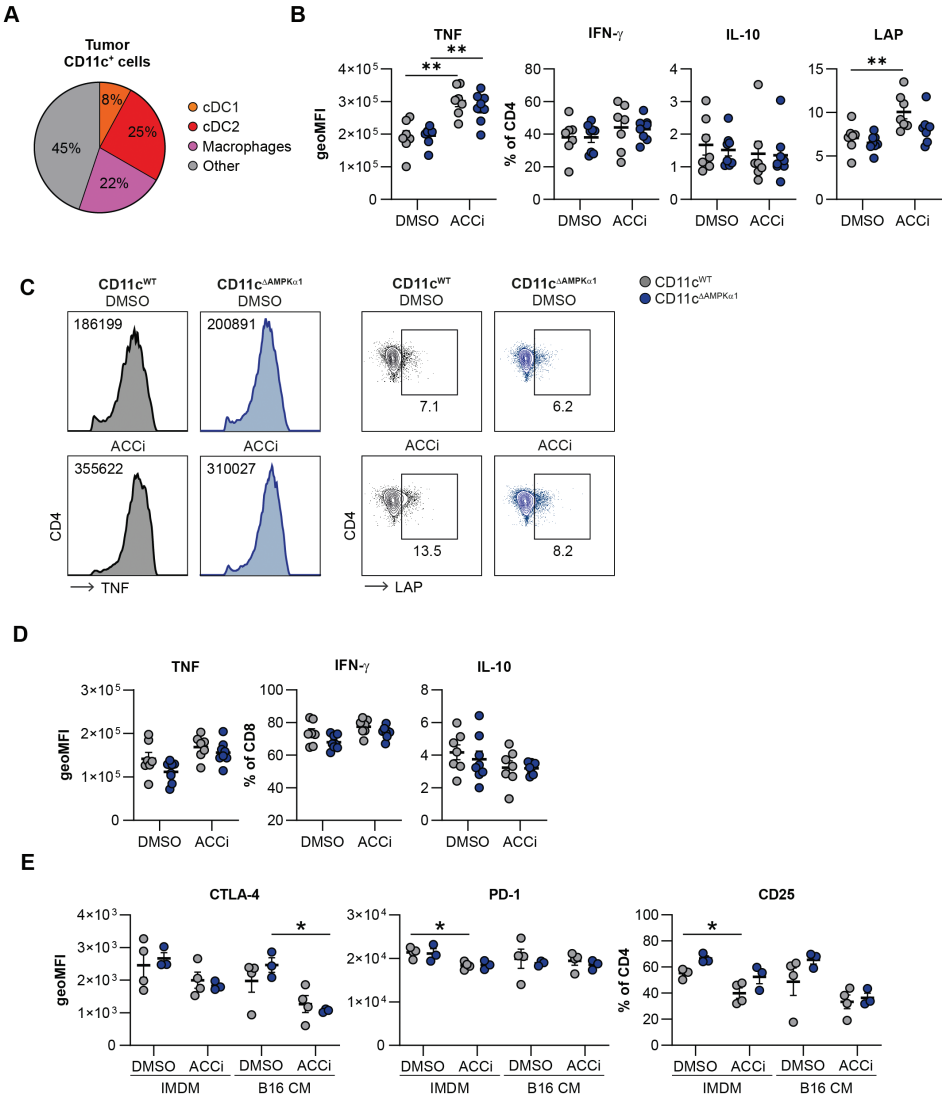

Supplementary figure 5: ACC expression in DCs suppresses TNF and LAP levels in CD4⁺ T cells after *ex vivo* priming. A: Cell distribution within CD11c⁺ cells. **B-D:** After 8 days of DC-T cell co-culture, cells were restimulated with PMA and ionomycin in presence of Brefeldin A. Cytokine levels and representative lots of TNF and LAP expression by (**B,C**) CD4⁺ OT-II T cells and (**D**) CD8⁺ OT-I T cells. **E:** Expression levels of CTLA-4, PD-1, and CD25 by CD4⁺ T cells after 3 day co-culture with sorted cDC2s. Results are expressed as means ± SEM. Statistical analyses were performed using two-way Anova with Tukey post-hoc test. *p < 0.05, **p < 0.01.

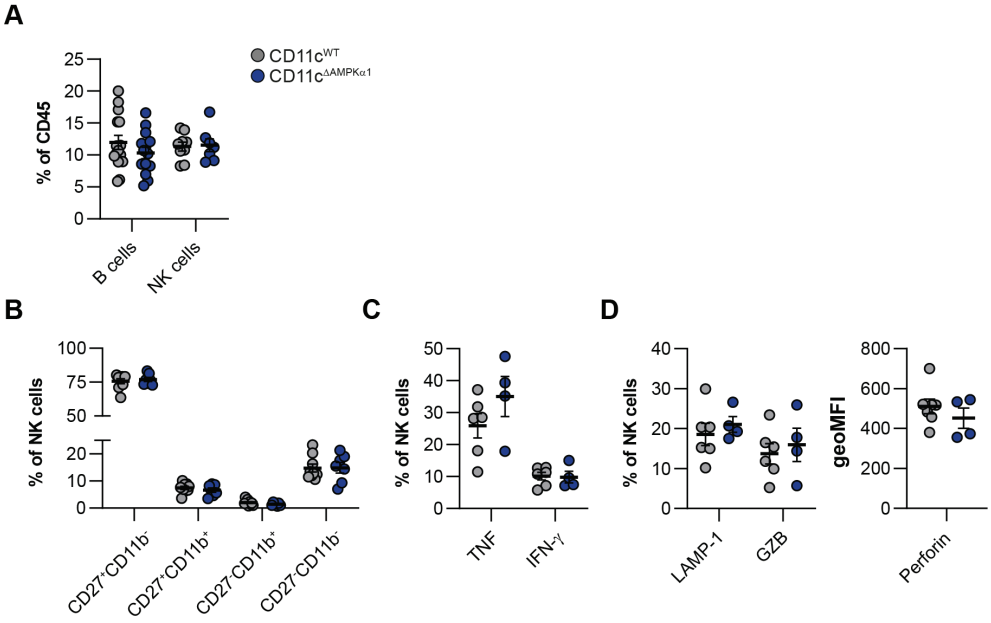

Supplementary figure 6: No differences in intra-tumoral NK cells between CD11c^{WT} and CD11c$^{\Delta AMPK\alpha1}$ mice. A: Frequencies of total B cells and NK cells. **B:** Frequencies of different NK cell subsets based on CD27 and CD11b expression. **C:** cytokine levels after PMA and ionomycin restimulation in the presence of Brefeldin A. **D:** Expression levels of cytotoxicity markers. LAMP-1 was added during restimulation with PMA/ionomycin in presence of Brefeldin A and granzyme B and perforin were stained intracellularly. Results are expressed as means ± SEM. Statistical analyses were performed using unpaired t-test. *p < 0.05, **p < 0.01.